University of Cincinnati

Date: 1/20/2011

I, Ruirong Shi , hereby submit this original work as part of the requirements for the degree of Master of Science in Electrical Engineering.

It is entitled:

Zeroth-Order Resonator (ZOR) Antenna Using Composite Right/Left-Handed (CRLH) Microstrip Transmission Line (TL)

Student's name: **Ruirong Shi**

This work and its defense approved by:

Committee chair: Altan Ferendeci

Committee member: Marc Cahay

Committee member: Peter Kosel

1316

Zeroth-Order Resonator (ZOR) Antenna Using Composite Right/Left-Handed (CRLH) Microstrip Transmission Line (TL)

A thesis submitted to

Graduate School

of University of Cincinnati

in partial fulfillment of

the requirement for the degree of

MASTER OF SCIENCE

OF ELECTRICAL ENGINEERING

in the Department of

Electrical and Computer Engineering

Of the College of Engineering & Applied Science

by

Ruirong Shi

Jan. 2011

Committee Chair:

Dr. Altan M. Ferendeci

Abstract

Left-handed materials are artificial materials that have negative permittivity and negative permeability simultaneously, which provide unique new properties in comparison with the traditional right-handed (RH) materials.

Composite Right/Left-Handed (CRLH) transmission line (TL) structure, which is composed of the series interdigital capacitor and the shunt inductor, is fabricated to implement the left-handed properties in reality. In this thesis, the CRLH TL theory is interpreted carefully. The verification is done by the ADS momentum simulation. The good agreement between the theoretical expectation and the simulation results is observed.

Zeroth-order resonator (ZOR) CRLH antenna has a unique characteristic that its resonate frequency is independent on the its physical length. Thus small compact antennas can be produced.

The ZOR CRLH antennas operating at 915-MHz are designed, simulated, fabricated and tested. A systematic method to fabricate the ZOR CRLH antenna is introduced. The characteristics of the ZOR antenna are further researched.

Acknowledgments

I wish to express my sincere thanks to my advisor, Dr. Altan M. Ferendeci. During my graduate study in University of Cincinnati, his patience, guidance, knowledge, inspiration, and encouragement give me a lot of help to finish this thesis.

Specially, I sincerely thank my parents, who have encouraged me to study abroad for long. That is the reason why I came to USA. At the same time, I also want to thank my siblings. They all gave me great encouragement and support while I was studying in University of Cincinnati.

Also, many thanks go out to all the members of Microwave and Millimeter Wave Electronics Lab, Jian Xu, Piyou Zhang, Yuanzhi Lin, Qingyi Wu, and Weiqun Chen. Their assistance, discussion, and encouragement make me a better life in this country.

I also want to express my sincere appreciation to all my friends in Cincinnati and other places. Some of them encouraged and helped me a lot, and some gave me valuable advice. I apologize that I can't list all of them.

Table of Content

List of Figures

Chapter 1

Introduction

1.1 Metamaterials

Metamaterials are artificial structures that can be designed with unusual properties not readily available in nature [1][2].

Left-Handed Materials (LHM) are materials that exhibit negative permittivity (ε) and negative permeability (μ) at the same time. In fact, these materials are designated and used in the terms of doubly negative materials or negative index materials. In 1968 the term "left-handed material" was first theorized by a prediction of Russian theorist V. G. Veselago[3].

Recently, the term metamaterial has been used most often in reference to left-handed structures in many references [1][2]. Since the LH structures are artificial, they are homogenous, and simultaneously have negative permittivity and permeability.

It should be noted that metamaterials may compass a much broader range of structures. However, LH structures have been so far the most popular one, due to their exceptional property of having negative permittivity (ε) and negative permeability (μ).

1.2 Left-Handed Materials

In 1968, Russian physicist Veselago first theorized the LHMs concept [3]. In his paper, the possible existence of LHM is predicted and their corresponding electromagnetic properties are also speculated, such as the both reversal of the Snell's Law and the Doppler Effect. As a result, LHMs support the antiparallel electromagnetic waves, or the backward wave, which means that the electromagnetic wave are moving in the opposite direction to the flow of the energy. [4].

In 2001, experiments made by a group at University at California, San Diego (UCSD), verified the theory of LHMs for the first time[5]. They built the material, which we can refer to as negative refractive index (NRI) metamaterial, with an array of loosely coupled resonant cells. Each cell is composed of thin wire strips and split ring resonators (SRRs), which provides the negative permittivity and the negative permeability simultaneously. The SRRs sample of their experiments is shown in Fig. 1.1.

Fig.1.1 The split-ring resonators (SRRs) sample of UCSD's[5]

Repeated experiments confirmed UCSD's finding [6] and additional research were continued [7]-[9]. However, due to the lossy and narrow-banded characteristics, they are hard to implement in the range of microwave frequencies.

Soon the transmission line (TL) approach of LHMs, CRLH TL structures appeared [10], [11]. The new approach is implemented on non-resonant structures with lower loss and wider bandwidth. Another advantage of TL approach is that they are in planar configurations, which are compatible with modern microwave integrated circuits (MICs). Finally TL approach can benefit from the efficient and well-established TL theory for efficient design for microwave applications.

1.3 New Antenna Design

A new type of resonant microstrip antenna – the Zeroth-Order Resonant (ZOR) antenna based on CRLH TLS has been developed [12]. The ZOR antenna requires much smaller physical size in comparison with the traditional microstrip rectangular antenna. Additional improvements were made on the ZOR antennas [13][14][15].

This thesis work is devoted to the CRLH TL and ZOR antenna development around 915 MHz for RFID applications. Theory and method to the design of the ZOR CRLH antenna will be introduced. Experiments are done to verify this theory. The ZRO CRLH antennas were designed and their characteristics are researched. Further research direction will be provided.

References

[1] A. Lai, C. Caloz, and T. Itoh, “Composite Right/Left-handed Transmission Line Metamaterials”, IEEE Microwave Magazine, pp. 34-50, September 2004

[2] C. Caloz and T. Itoh, Electromagnetic Metamaterials: Transmission Line Theory and Microwave Applications. New York: Wiley, 2004.

[3] V. Veselago, “The electrodynamics of substances with simultaneously negative values of ε and μ,” Soviet Physics Uspekhi, vol. 10, no. 4, pp. 509–514, 1968.

[4] S.A. Shelby, D.R.Smith and S. Schultz, “Experimental verification o a negative index of refraction,” Science, vol.292, no. 5541, pp 77-79,2001.

[5] R. A. Shelby, D.R. Smith, and S. Schultz, “Experimental verification of a negative index of refraction,” Science, vol. 292, no. 5514, pp.77–79, 2001.

[6] A. A. Houck, J. B. Brock, and I.L. Chuang, “Experimental observations of a left-handed material that obeys Snell's Law,” Phys. Rev.Lett., vol. 90, pp. 137–401, Apr. 2003.

[7] C. R. Simovski, P. A. Belov, and H. Sailing, “Backward wave region and negative material parameters of a structure formed by lattices of wires and split-ring resonators,” IEEE Trans. Antennas Propagat., vol. 51, pp. 2582–2591, Oct. 2003.

[8] E. Ozbay, K. Aydin, E. Cubukcu, and M. Bayindir, “Transmission and reflection properties of composite double negative metamaterials in free space,” IEEE Trans. Antennas Propagat., vol. 51, pp. 2592–2595, Oct. 2003.

[9] R. W. Ziolkowski and A. D. Kipple, “Application of double negative materials to increase the power radiated by electrically small antennas,” IEEE Trans. Antennas Propagat., vol. 51, pp. 2626–2640, Oct. 2003.

[10] C. Caloz, H. Okabe, T. Iwai, and T. Itoh, “Transmission line approach of left-handed (LH) materials,” in Proc. USNC/URSI National Radio Science Meeting, San Antonio, TX, June 2002, vol. 1, p. 39.

[11] G. V. Eleftheriades, O. Siddiqui, and A.K. Iyer, “Transmission line models for negative refractive index media and associated implementations without excess resonators,” IEEE Microwave Wireless Compon. Lett., vol. 13, pp. 51–53, Feb. 2003.

[12] A. Sanada, C. Caloz, and T. Itoh, “Zeroth order resonance in composite right/left-handed transmission line resonators,” in Proc. Asia-Pacific Microwave Conf., vol. 3, pp. 1588–1592. Seoul, Korea, 2003.

[13] A. Sanada, K.Murakami, I.Awai, C. Caloz, and T. Itoh, “ A planear zeroth-order resonator antenna using a left-handed transimission line,” in Proc. European Microwave Conf. pp.1341-1344, Amsterdam, Nerherlands, Apr. 2004.

[14] A.Sanada, K.Murakami, S.Aso, H.Kubo, and I.Awai, “A via-free microstrip left-handed transmission line,” IEEE MTT-S Digest, pp.301-304, Fort Worth, Jun.2004.

[15] C. J. Lee, K.M.K.Leong, and T. Itoh, “Composite right/left-handed transmission line based compact resonant antenna for RF module integration,” IEEE Trans. Antennas Propagat., vol. 54, pp. 2283–2291 Aug. 2006.

Chapter 2
Composite Right /Left Handed (CRLH) Transmission Line (TL)

2.1 Composite Right/Left-handed Transmission Line Approach

Composite Right/left-handed (CRLH) metamaterials are the metamaterials with both of the right-handed (RH) properties and the left-handed (LH) properties [1]. The CRLH metamaterials has been applied to some novel microwave devices.

2.1.1 Ideal Homogeneous TLs.

A homogeneous TL has invariant cross section along the direction of propagation. An effectively homogeneous structure is a structure whose structural aver-age cell size p is much smaller than the guided wavelength λ_g. Therefore, this average cell size should be at least smaller than a quarter of guided wavelength, $p < \lambda_g / 4$ [2].

The equivalent homogeneous transmission line modes for the purely RH, purely LH, and CRLH transmission lines are shown in Fig. 2.1.

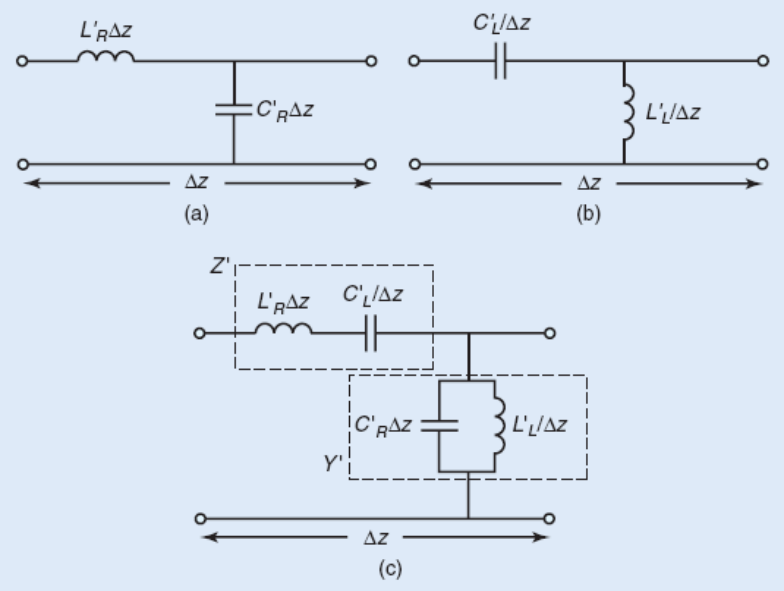

(a) Purely homogeneous RH TL.(b) Purely homogeneous LH TL. (c) CRLH TL.

Fig.2.1 Equivalent circuit models[1]

In Fig. 2.1, the purely RH TL consists of a series inductance and a shunt capacitance per-unit length, while the purely LH consists of a series capacitance and a shunt inductance. Naturally, the purely RH TL and LH TL actually do not exist because of the parasitic inductances and capacitances. So the CRLH TL structure is the most general form of a TL structure with LH attributes. The general CRLH TL structure is a combination of a series inductance L_R' and capacitance C_L' with a shunt capacitance C_R' and inductance L_L'.

2.1.2 Fundamental Characteristics of the CRLH TLs.

Generally, a loss-less CRLH TL model is a combination of a series inductance L_R' capacitance C_L' with a shunt capacitance C_R' and inductance L_L'.

For the case of CRLH TL,

$$Z'(\omega) = j\omega L'_R + \frac{1}{j\omega C'_L}$$
$$Y'(\omega) = j\omega C'_R + \frac{1}{j\omega L'_L} \qquad (2.1)$$

where Z' and Y' are the impedance and the admittance per-unit length of the CRLH transmission line.

The complex propagation constant γ of the transmission line can be expressed as

$$\gamma = \alpha + j\beta = \sqrt{Z'Y'} \qquad (2.2)$$

For convenience, we introduce the variables:

$$\omega_R' = \frac{1}{\sqrt{L_R'C_R'}}$$
$$\omega_L' = \frac{1}{\sqrt{L_L'C_L'}} \qquad (2.3)$$
$$k = L_R'C_L' + L_L'C_R'$$

and the series and shunt resonant frequencies

$$\omega_{se} = \frac{1}{\sqrt{L_R'C_L'}}$$
$$\omega_{sh} = \frac{1}{\sqrt{L_L'C_R'}} \qquad (2.4)$$

The transition frequency is defined by

$$\omega_0 = \sqrt{\omega_R' \omega_L'} = \frac{1}{\sqrt[4]{L_R' C_R' L_L' C_L'}} \tag{2.5}$$

Therefore the dispersion relation for homogenous CRLH TL is

$$\gamma = \alpha + j\beta = js(\omega)\sqrt{(\frac{\omega}{\omega_R'})^2 + (\frac{\omega_L'}{\omega})^2 - k\omega_L'^2} \tag{2.6}$$

Where $s(\omega)$ has the following sign function

$$s(\omega) = \begin{cases} -1 \quad if \quad \omega < \min(\omega_{se}, \omega_{sh}) \quad LH \quad range \\ +1 \quad if \quad \omega > \min(\omega_{se}, \omega_{sh}) \quad RH \quad range \end{cases} \tag{2.7}$$

The propagation constant γ can be purely real or purely imaginary depending on whether the radicand is positive or negative, respectively. In the frequency range where β is purely real, the electromagnetic fields will pass the CRLH transmission line without loss since $\gamma = j\beta$. In the frequency range where β is purely imaginary, then the CRLH is in a stop-band range because $\gamma = \alpha$ is a real number.

The group velocity and the phase velocity can be obtained from

$$\begin{aligned} v_g &= \frac{\partial \omega}{\partial \beta}, \quad Group \ \ velocity \\ v_p &= \frac{\omega}{\beta}, \quad Phase \ \ velocity \end{aligned} \tag{2.8}$$

Fig.2.2 shows the $\omega - \beta$ or dispersion diagram of a pure RH TL, pure LH TL, CRLH TL, respectively. These diagrams show that the group velocity and the phase velocity for the pure RH TL have the same direction because $v_g v_p > 0$, while the group velocity and the phase velocity for the pure LH TL have the opposite directions since $v_g v_p < 0$.In addition, the CRLH TL's dispersion diagram shows that it has an LH and RH region.

The propagation constant of a material is $\beta = nk_0 = n\omega / c$, where the refractive index of the material $n = \pm\sqrt{\mu_r \varepsilon_r}$ and the speed of light in the free space $c = 1/\sqrt{\mu_0 \varepsilon_0}$. In a word, we could get $\beta c = n\omega$. For a pure RH material, $n > 0$. and for a pure LH material, $n < 0$.

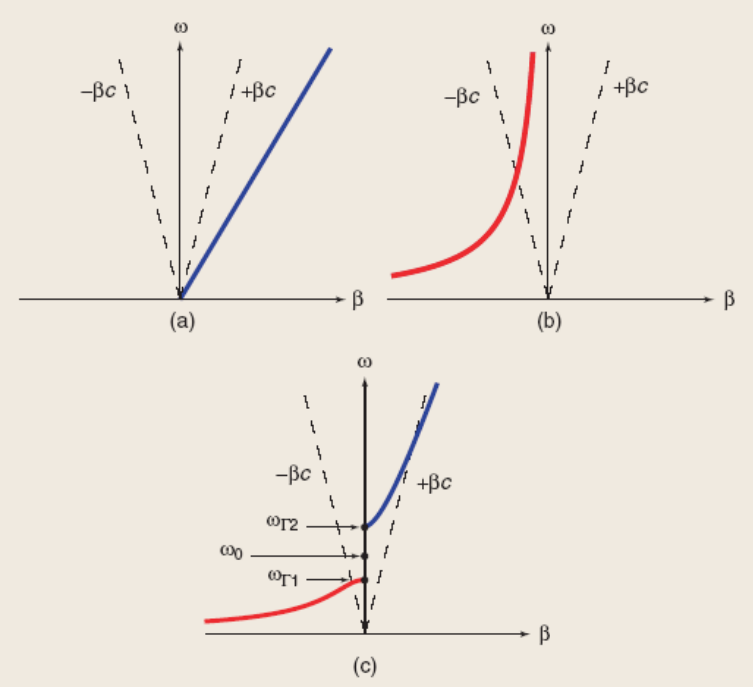

(a) Purely homogeneous RH TL. (b) Purely homogeneous LH TL.

(c) CRLH TL (unbalanced) .

Fig.2.2 Dispersion diagrams corresponding to the TLs of Fig. 2.1[1].

The CRLH TL characteristics impedance can be obtained from

$$Z_C = \sqrt{\frac{Z'}{Y'}} = Z_L \sqrt{\frac{(\omega/\omega_{se})^2 - 1}{(\omega/\omega_{sh})^2 - 1}} \qquad (2.9)$$

where Z_L is the pure LH impedance

$$Z_L = \sqrt{\frac{L_L'}{C_L'}} \tag{2.10}$$

and similarly the pure RH impedance

$$Z_R = \sqrt{\frac{L_R'}{C_R'}} \tag{2.11}$$

2.1.3 Balanced and Unbalanced Resonances.

The CRLH TL exhibits interesting properties in the particular case where the series and shunt resonant frequencies (2.4) are equal

$$\omega_{se} = \omega_{sh} \tag{2.12a}$$

or equivalently

$$L_R' C_L' = L_L' C_R' \tag{2.12b}$$

or equivalently

$$Z_L = Z_R \tag{2.12c}$$

where Z_L and Z_R were defined in Eqn. (2.9) and (2.10). This case is called balanced case and is opposed to the general unbalanced case, where the series and shunt resonances are different

$$\omega_{se} \neq \omega_{sh} \tag{2.13}$$

For the unbalanced case, impedance conditions correspond to zero velocities ($v_g = 0$) or zero slopes in the dispersion diagram, i.e., TL resonances, and result in the emergence

of a stop band or gap, despite the assumed absence of loss. Assuming ports with constant and real impedances, the characteristic impedances of the unbalanced case are

$$Z_C[0 < \omega < \min(\omega_{se}, \omega_{sh})] \in real \quad (LH \quad passband)$$
$$Z_C[\min(\omega_{se}, \omega_{sh}) < \omega < \max(\omega_{se}, \omega_{sh})] \in image \quad (el. \quad or \quad mag.gap) \quad (2.14)$$
$$Z_C[\omega > \max(\omega_{se}, \omega_{sh})] \in real \quad (RH \quad passband)$$

In the balanced case, the characteristic impedance became a frequency-independent quality.

$$Z_C = Z_L = Z_R \quad (2.15)$$

This means that the balanced condition allows matching over an infinite bandwidth. At the same time, the propagation constant in (2.6) could reduce to the simple expression

$$\beta = \beta_R + \beta_L = \omega\sqrt{L_R' C_C'} - \frac{1}{\omega\sqrt{L_L' C_L'}} \quad (2.16)$$

The balanced CRLH TL has a number of advantages over the unbalanced CRLH TL, which may be summarized as following [2]:

- Its model is simpler than that of the general unbalanced model of Fig.2.1(c) because series combined LH and RH contributions are decoupled from each other, as shown in Fig.2.3.(a).
- In contrasted to the unbalanced TL, the balanced TL has no stop band. This is shown in Fig.2.3.(b).
- The characteristic impedance of the balanced TL is a constant frequency independent quantity.

- A unique feature of CRLH structure is nonzero velocity at the transition frequency.
- Because the transition frequency ω_0 associated with the fundamental mode, it supports wave propagation ($\upsilon_g \neq 0$) with $\beta = 0$ and it is called the phase origin of the CRLH TL. At this frequency, the phase shift along a line of length l is zero, $\phi = -\beta l = 0$. When frequency is decreased below ω_0 toward zero, the phase becomes positive, increases progressively, and tends to infinity as $\phi(\omega \to 0) = -\beta l \to +\omega_L' l / \omega$. When the frequency is increased above ω_0 toward infinity, the phase becomes negative, increases progressively in magnitude, and tends to infinity as $\phi(\omega \to 0) = -\beta l \to -\omega_L' l / \omega$.
- At the transition frequency, the guided wavelength is infinite and the electrical length of the line is zero.

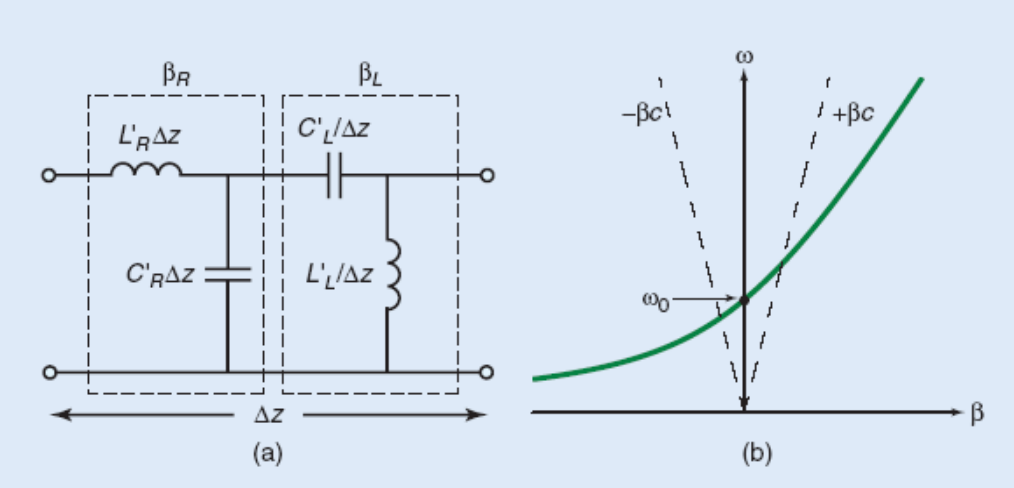

(a) Equivalent circuit model.

(b) Dispersion diagram showing seamless LH to RH transition.

Fig. 2.3 Balanced form of Fig. 2.1(c)[1].

2.2 LC-Based CRLH Transmission Line

The ideal CRLH TL is not readily available from nature, but an effectively homogenous CRLH TL operative in a restricted frequency range of the passband can be realized in the form of a ladder network circuit structure.

The network is obtained by cascading the LC unit cell shown in Fig.2.4 (a) so as to obtain the ladder network shown in Fig.2.4 (b). Cascading N number of LC unit cells results in a TL equivalent to an ideal CRLH TL of length l under the condition $p \to 0$. This is called the homogeneity condition because it ensures that the artificial TL is equivalent to the ideal homogenous TL. In practice, this condition can be translated into the rule-of –thumb effective-homogeneity conditions, $p<\lambda_g/4$, introduced in Section 2.1.

Under these conditions, resulting applications are published in [3][4][5].

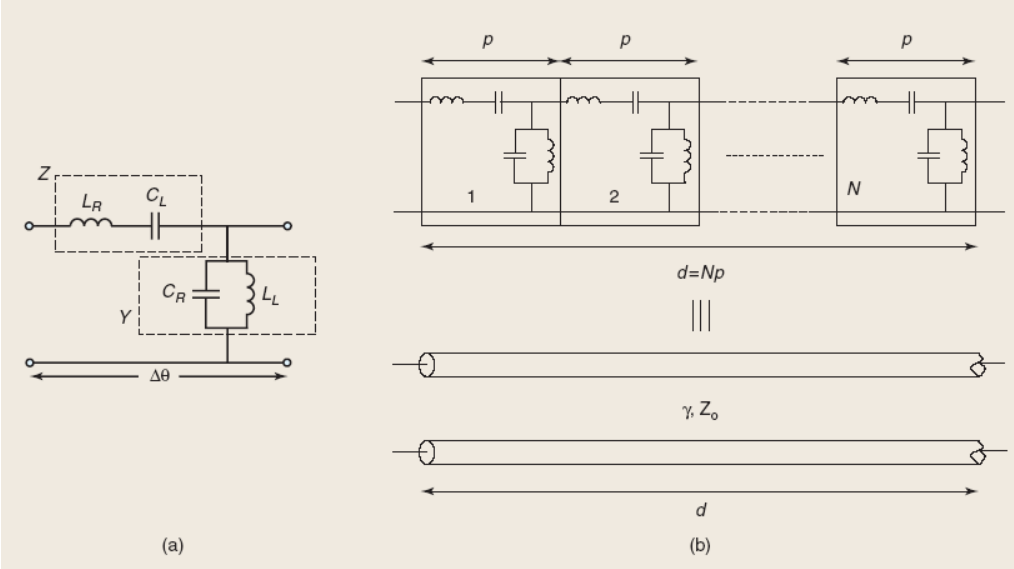

(a) Unit cell of CRLH (b) Periodic network equivalent to a homogeneous CRLH TL

Fig. 2.4 LC-based CRLH TL [1].

2.3 Zeroth-Order Resonator (ZOR)

2.3.1 Principal of ZOR

For the pure RH distributed resonator, the resonance frequencies are determined by the physical length l of the structure and is a multiple of half a wavelength or, equivalently, the electrical length $\theta = \beta l$ is a multiples of π,

$$l = n\frac{\lambda}{2} \quad \theta_n = \beta_n l = (\frac{2\pi}{\lambda}) \bullet (\frac{n\lambda}{2}) = n\pi \tag{2.17}$$

with $n = +1,+2,\cdots + \infty$

In contrast to the pure RH TL, an ideal homogenous balanced CRLH TL can have $\beta = 0$ and $\beta < 0$, as shown in Fig.2.10. Therefore, the electrical length $\theta = \beta l$ can be zero and negative, which means that the resonance index m becomes symmetrically defined around $n = 0$. Thus

$$l = \mid n \mid \frac{\lambda}{2} \quad \theta_n = \beta_n l = (\frac{2\pi}{\lambda}) \bullet (\frac{n\lambda}{2}) = n\pi \tag{2.18}$$

with $n = 0,+1,+2,\cdots + \infty$

The CRLH TL resonator has several differences compared with the pure RH TL resonator:

- Negative resonances ($n < 0$) and ($n = 0$) exist in addition to the conventional positive resonances ($n > 0$), as shown in Fig 2.5(a).
- Except for the mode $n = 0$, each mode has a corresponding mode with the opposite sign with identical field distribution. Therefore, each pair should have identical

impedance but different bandwidth due to the dissymmetry of the CRLH dispersion curve, as shown in Fig 2.5(a).

- Due to the nonlinear nature of the CRLH dispersion curve, especially in the LH range, the resonant frequencies are not harmonic ratios as shown in Fig 2.5(a).
- The $n = 0$ mode is not related to the physical length of TL: this mode corresponds to an infinite wavelength. At this mode, the voltage distribution along the TL is the flat field distribution, as shown in Fig 2.5(b).

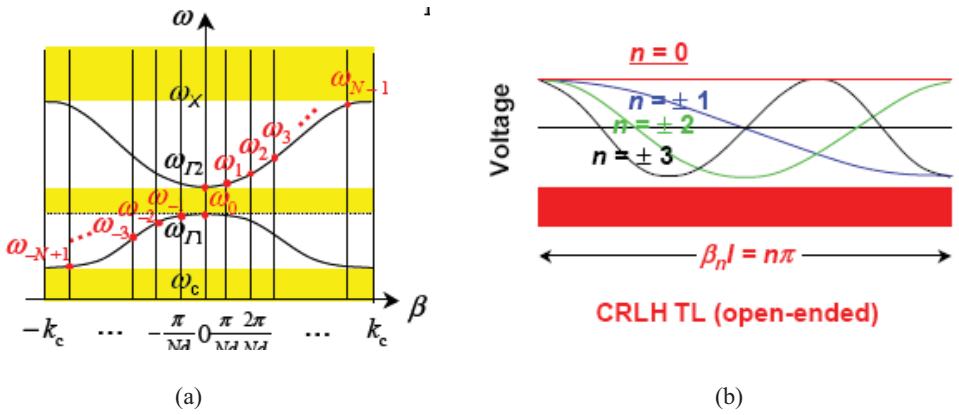

(a) (b)

Fig.2.5 CRLH TL resonator. (a) Dispersion relation of the CRLH TL and resonance frequencies. (b) Typical field distribution of resonance modes [6].

2.3.2 ZOR Characteristics

From the Eq. (2.9), it is clear that the balanced CRLH TL structure has no gap between the LH and the RH range when it is in the propagating TL operation with good matching. If the CRLH TL is unbalanced, it exhibits two resonance frequencies ω_{se} and ω_{sh}, where it is terminated by matched load. What will happen if the line is open-ended or short-ended?

In the open-ended case, the input impedance Z_{in} seen from one end of the resonator toward the other end is given by [2]

$$\begin{aligned} Z_{in}^{open} &= -jZ_C \cot(\beta l) \overset{\beta \to 0}{=} -jZ_C \frac{1}{\beta l} \\ &= -j\sqrt{\frac{Z'}{Y'}}\left(\frac{1}{-j\sqrt{Z'Y'}}\right)\frac{1}{l} = \frac{1}{Y'l} = \frac{1}{Y'(Np)} \end{aligned} \tag{2.19}$$

where N is the number of unit cell, and Y' is the admittance of the CRLH unit cell, given by Eqn.(2.1). This result shows that the input impedance of an operation is $1/N$ times the impedance of the anti-resonant L_L/C_R shunt tank. Because N is a simple integer, not affecting the susceptance, the resonance of the whole resonator is the same as resonance of the admittance. Therefore, there is a single resonance frequency,

$$\omega_{res}^{open} = \omega_{sh} = \frac{1}{\sqrt{L_L C_R}} \tag{2.20}$$

In contrast, no resonance occurs at $\omega_{se} = 1/\sqrt{L_R C_L}$.

In the short-ended case, the impedance of Z_{in} seen from one end of the resonator toward the other end is given by [2]

$$\begin{aligned} Z_{in}^{short} &= jZ_C \tan(\beta l) \overset{\beta \to 0}{=} -jZ_C \beta l \\ &= -j\sqrt{\frac{Z'}{Y'}}\left(j\sqrt{Z'Y'}\right)\frac{1}{l} = Z'l = Z'(Np) \end{aligned} \tag{2.21}$$

where N is the number of unit cell, and Z' is the admittance of the CRLH TL unit cell, given by Eqn.(2.1). The result shows that the input impedance of an open-ended is N times the impedance of the resonant L_R/C_L shunt tank. Since N is a simple integer,

not affecting the reactance, the resonance of the whole resonator is the same as the resonance of the series impedance.

$$\omega_{res}^{short} = \omega_{se} = \frac{1}{\sqrt{L_R C_L}} \tag{2.22}$$

In contrast, no resonance occurs at $\omega_{sh} = 1/\sqrt{L_L C_R}$.

In the particular case of balanced resonance, the zeroth-order resonance occurs for both the open-ended and the short-ended resonators, since $\omega_0 = \omega_{se} = \omega_{sh}$.

The remarkable feature of zeroth-order resonator is that, either for an open-ended or a short-ended configuration, the resonance frequency depends only on the circuit elements L_L/C_R or L_R/C_L of the unit cell and not the physical length l of the resonator. This suggests that a zeroth-order resonator could be made arbitrarily small, the limitation in size reduction being the minimum footprint by the LC elements for the required LC values in a given technology.

2.3.3 Microstrip Realization

In 2003, the first ZOR in CRLH TL resonator is reported [6]. An open-ended CRLH TL resonator is implemented in microstrip technology, as shown in Fig.2.6.

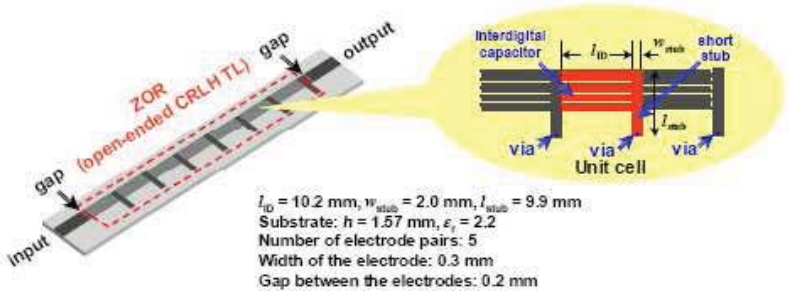

(a) Prototype of the resonator

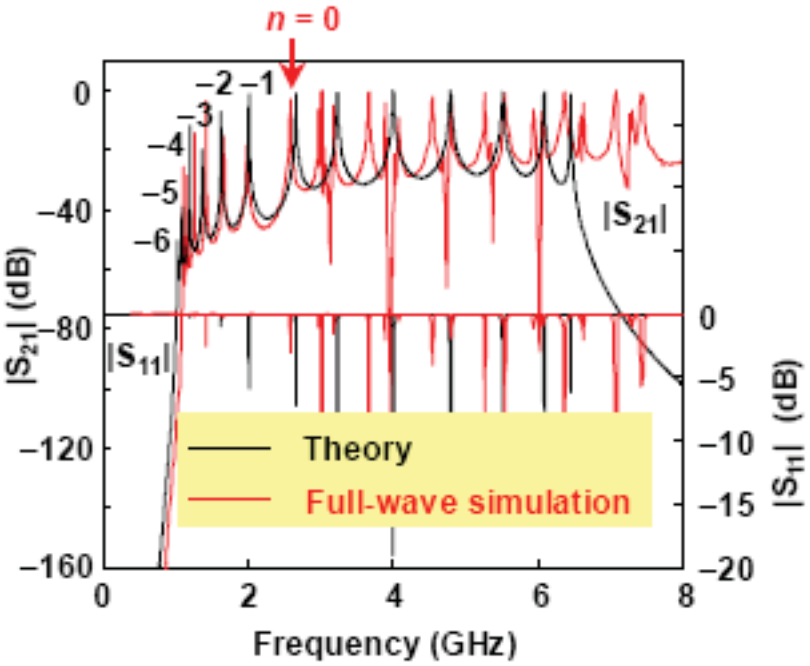

(b) Transmission and reflection parameters of ZOR(the upper plot is S_{21} paramenters and the middle plot is the S_{11} paramenters).

Fig.2.6 The 7-cell CRLH TL resonator [6]

Later, a via-free microstrip CRLH TL antenna was proposed [7][8]. The metal patch replaces the via to connect to the ground. The metal patch provides capacitance C_g to

the ground. When C_g is large, it provides the virtual ground voltage. Thus the virtual ground leads to a little change of the resonant frequencies, as shown in Fig.2.7.

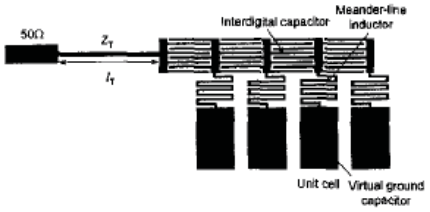

(a) Circuit pattern.

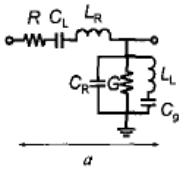

(b) Equivalent circuit of the unit cell

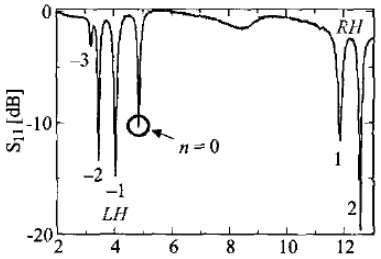

(c) Measurement $|S_{11}|$ of antenna.

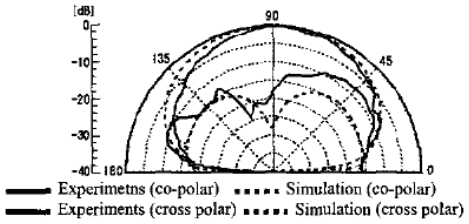

(d) Measurement radiation patterns.

Fig.2.7 The via-free ZOR CRLH TL antenna [7]

At the same time, research shows when optimally matched to the air impedance the balanced CRLH TL can be used as an efficient, frequency-scanned leaky-wave antenna [9]. A 30-cell leaky-wave antenna structure, incorporating both series and shunt varactors for optimal impedance matching and maximal tuning was reported [10].

The CRLH TL realized by interdigital capacitor and short stub cannot provide a large series capacitance and inductance in small area. Several electrically small CRLH antennas based on the modified mushroom structure was reported [11]. As shown in Fig.2.8, a metal insulator metal (MIM) with high dielectric constant and thin substrate

height can increase C_L .The inductance L_L is realized by a metallic via with additional CPW stub connected to the ground. The via length and CPW length can be enlarged to increase the shunt inductance. A small unit cell can be developed by combining the MIM capacitor and via plus CPW stub with large values of C_L and L_L .

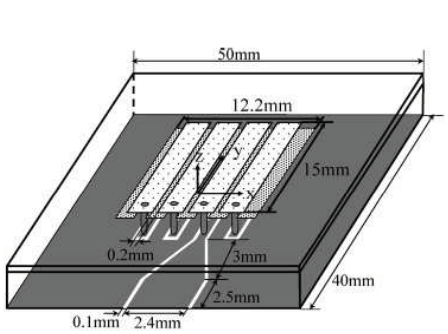

(a) Configuration of the small antenna

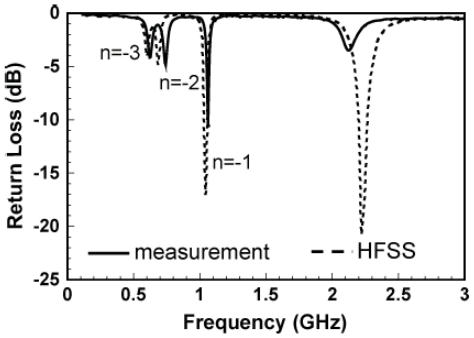

(b) Return loss of the small antenna

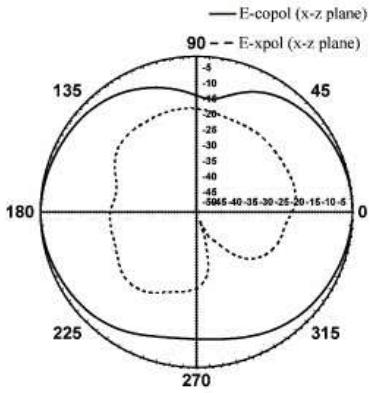

(c) Measured radiation pattern in E-plane

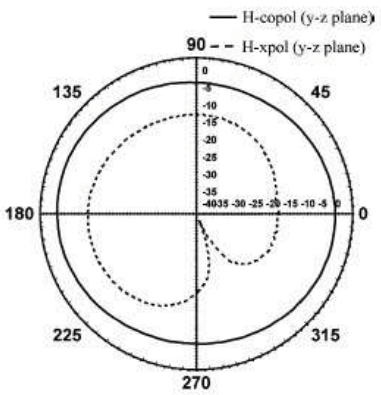

(d) Measured radiation pattern in H-plane

Fig.2.8 The electrically small resonant antenna [11].

Reference:

[1] A. Lai, C. Caloz, and T. Itoh, "Composite Right/Left-handed Transmission Line Metamaterials", IEEE Microwave Magazine, pp. 34-50, September 2004

[2] C. Caloz and T. Itoh, Electromagnetic Metamaterials: Transmission Line Theory and Microwave Applications. New York: Wiley, 2004.

[3] I. H. Lin, M. De Vincetis, C. Caloz, and T. Itoh. "Arbitrary dual-band components using composite right/left-handed transmission line", IEEE Trans. Microwave Theory Tech., vol. 52, pp.1142–1149, Apr. 2004.

[4] C. Caloz, A.Sanada, and T.Itoh, "A novel composite right-/left-handed coupled-line directional coupler with arbitrary coupling level and broad bandwidth," IEEE Trans. Microwave Theory Tech., vol. 52, pp.980–992, Mar. 2004.

[5] A. Sanada, C. Caloz, and T. Itoh, "Planar distributed structures with negative refractive properties," IEEE Trans. Microwave Theory Tech., vol. 52, pp. 1252–1263, Apr. 2004.

[6] A. Sanada, C. Caloz, and T. Itoh, "Zeroth order resonance in composite right/left-handed transmission line resonators," in Proc. Asia-Pacific Microwave Conf., vol. 3, pp. 1588–1592. Seoul, Korea, 2003.

[7] A. Sanada, K.Murakami, I.Awai, C. Caloz, and T. Itoh, " A planear zeroth-order resonator antenna using a left-handed transimission line," in Proc. European Microwave Conf. pp.1341-1344, Amsterdam, Nerherlands, Apr. 2004.

[8] A.Sanada, K.Murakami, S.Aso, H.Kubo, and I.Awai, "A via-free microstrip left-handed transmission line," IEEE MTT-S Digest, pp.301-304, Fort Worth, Jun.2004.

[9] L.Liu, C. Caloz, and T. Itoh, “Dominant mode (DM) leaky-wave antenna with backfire- to-endfire scanning capability,” Electron. Lett., vol.38, no.23, pp 1414-1416, 2000.

[10] S.Lin, C.Caloz, and T. Itoh, “Metamaterial-based electronically controlled transmission-line structure as a novel leaky-wave antenna with tunable radiation anle and beamwidth,” IEEE Trans. Microwave Theory Tech., vol. 53, pp.161–173, Jan. 2005.

[11] C. J. Lee, K.M.K.Leong, and T. Itoh, “Composite right/left-handed transmission line based compact resonant antenna for RF module integration,” IEEE Trans. Antennas Propagat., vol. 54, pp. 2283–2291 Aug. 2006.

Chapter 3

Verification of the CRLH TL

3.1 Microstrip Unit Cell Model

There are many technologies to implement the artificial CRLH TL, as presented in Chapter 2. Here we consider adapting the 1-D CRLH microstrip TL structure, which is implemented on the microstrip TL with interdigital capacitors and stub inductor connected to the ground plane. A unit cell of 1-D microstrip CRLH TL is shown in Fig.3.1(a). Because this structure is based on the distributed components and therefore compatible with the microwave monolithic integrated circuit (MMICs) technologies, it has attracted a lot of attention in the scientific community [1]-[4].

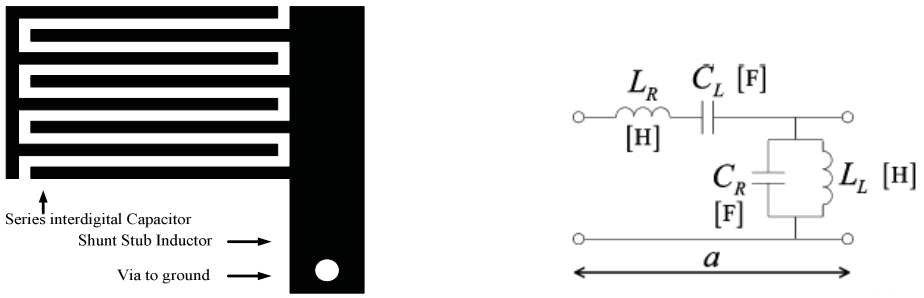

(a) Unit cell of 1-D microstrip CRLH TL (b) Equivalent circuit model

Fig. 3.1 Unit cell of 1-D microstrip CRLH TL

The unit cell of microstrip CRLH TL consists of the interdigital capacitors and stub inductor shorted to the ground plane by the via. This unit cell can be accurately mapped to the model of Fig.3.1(b) with the help of Fig.3.2.

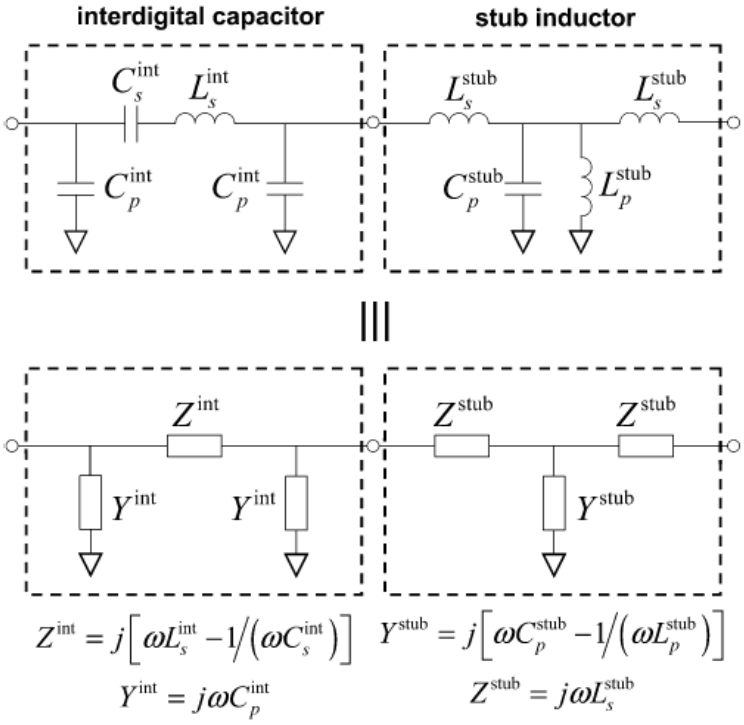

Fig. 3.2 Equivalent-circuit models for the circuit model

of the microstrip unit cell shown in Fig. 3.1.(b).

The equivalent T and Π networks of these two components can be characterized by the following admittance and impedance matrices [1][4]:

$$\left[Y^{\text{int}}\right] = \begin{bmatrix} Y_{11}^{\text{int}} & Y_{12}^{\text{int}} \\ Y_{21}^{\text{int}} & Y_{22}^{\text{int}} \end{bmatrix} = \begin{bmatrix} \frac{1}{Z^{\text{int}}} + Y^{\text{int}} & -\frac{1}{Z^{\text{int}}} \\ -\frac{1}{Z^{\text{int}}} & \frac{1}{Z^{\text{int}}} + Y^{\text{int}} \end{bmatrix} \tag{3.1.a}$$

with
$$\begin{aligned} Z^{\text{int}} &= j[\omega L_s^{\text{int}} - 1/(\omega C_s^{\text{int}})] \\ Y^{\text{int}} &= j\omega C_p^{\text{int}} \end{aligned} \tag{3.1.b}$$

and

$$\left[Z^{stub}\right]=\begin{bmatrix} Z_{11}^{stub} & Z_{12}^{stub} \\ Z_{21}^{stub} & Z_{22}^{stub} \end{bmatrix}=\begin{bmatrix} \frac{1}{Y^{stub}}+Z^{stub} & \frac{1}{Y^{stub}} \\ \frac{1}{Y^{stub}} & \frac{1}{Y^{stub}}+Z^{stub} \end{bmatrix} \tag{3.2.a}$$

with

$$\begin{aligned} Y^{stub} &= j[\omega C_p^{stub} - 1/(\omega L_p^{stub})] \\ Z^{stub} &= j\omega L_s^{stub} \end{aligned} \tag{3.2.b}$$

Determination of the isolated inductances and capacitances in Eq. (3.1.b) and (3.2.b) is difficult, but the derivation with respect to ω provides one additional equation for the determination of all unknowns. The results are

$$\begin{aligned} C_p^{\text{int}} &= \frac{Y_{11}^{\text{int}} + Y_{21}^{\text{int}}}{j\omega} \\ L_s^{\text{int}} &= \frac{1}{2j\omega}\left(\omega\frac{\partial Z^{\text{int}}}{\partial\omega} + Z^{\text{int}}\right) \\ C_s^{\text{int}} &= \frac{2}{j\omega}\left(\omega\frac{\partial Z^{\text{int}}}{\partial\omega} - Z^{\text{int}}\right)^{-1} \end{aligned} \tag{3.3}$$

$$\begin{aligned} L_s^{stub} &= \frac{Z_{11}^{stub} + Z_{21}^{stub}}{j\omega} \\ C_p^{stub} &= \frac{1}{2j\omega}\left(\omega\frac{\partial Y^{stub}}{\partial\omega} + Y^{stub}\right) \\ L_p^{stub} &= \frac{2}{j\omega}\left(\omega\frac{\partial Y^{stub}}{\partial\omega} - Y^{stub}\right)^{-1} \end{aligned} \tag{3.4}$$

Finally, we obtain the four CRLH parameters:

$$\begin{aligned} L_R &= L_s^{\text{int}} + 2L_s^{stub} \approx L_s^{\text{int}} \\ C_R &= 2C_p^{\text{int}} + C_p^{stub} \\ L_L &= L_p^{stub} \\ C_R &= C_p^{\text{int}} \end{aligned} \tag{3.5}$$

The series inductance of the stub L_s^{stub} can be neglected, since it was found to be less than ten times smaller than the parasitic series inductance of interdigital inductance L_s^{stub}.

This procedure is more elaborate than a simple magnitude curve-fitting technique which may provide inaccurate results in terms of phase [1][4]

An important point to note is that the expressions for the extracted parameters depend on frequency, since Eqn. (3.3) and (3.4) are explicit functions of ω, as well as the Y and Z parameters. Consequently, a frequency at which extraction is performed, an extraction frequency ω_s must be chosen. If the whole bandwidth (LH and RH) of the CRLH structure is covered, a judicious choice for the extraction frequency is the transition frequency ω_0.

3.2 Design of Unit Cell of CRLH TL

To design a unit cell of CRLH TL is like a reverse procedure to extract the parameters of a unit cell of CRLH TL. The steps to design the unit cell of CRLH TL are listed here:

1. Decide the transition frequency f_0.For balanced CRLH TL design, the shunt and series frequency are equal, $f_{sh} = f_{se} = f_0$. For unbalanced CRLH TL design, there is a relation between three frequencies: $f_0 = \sqrt{f_{sh} f_{se}}$, then, choose appropriate shunt and series frequency.
2. Accord to the RH and LH impendance Eq. (2.10) and (2.11), choose appropriate values for the capacitors and inductances. If no appropriate value exist, repeat step 1.
3. Make an initial layout of the interdigital capacitor on the specific substrate. The Momentum simulation is done next to get the S parameters at the frequency center f_0 with $\pm 10\%$ bandwidth.
4. Change the S-parameters of the interdigital capacitor into Y-parameters at the

frequency center f_0 based on the two-port network parameters relation [5]:

$$
\begin{aligned}
Y_{11} &= Y_0 \frac{(1-S_{11})(1+S_{22})+S_{12}S_{21}}{(1+S_{11})(1+S_{22})-S_{12}S_{21}} \\
Y_{12} &= Y_0 \frac{-2S_{12}}{(1+S_{11})(1+S_{22})-S_{12}S_{21}} \\
Y_{21} &= Y_0 \frac{-2S_{21}}{(1+S_{11})(1+S_{22})-S_{12}S_{21}} \\
Y_{22} &= Y_0 \frac{(1+S_{11})(1-S_{22})+S_{12}S_{21}}{(1+S_{11})(1+S_{22})-S_{12}S_{21}}
\end{aligned}
\tag{3.6}
$$

5. Use the Eqn. (3.3) to get the results of $C_p^{\text{int}}, L_s^{\text{int}} \text{ and } C_s^{\text{int}}$. From the Eqn.(3.5), we can assume that C_p^{int} is the majority of the C_R .If necessary, adjust the gap, the finger length and the pair number of the interdigital capacitor, then repeat step 1 to 5 to get an appropriate capacitance value.
6. Make an initial layout of the stub inductor on the same substrate with the interdigital capacitor, then momentum simulation is done to get the S parameters.
7. Change the S-parameters of the stub inductor into Z-parameters based on the two-port network parameters relation [5] :

$$
\begin{aligned}
Z_{11} &= Z_0 \frac{(1+S_{11})(1-S_{22})+S_{12}S_{21}}{(1-S_{11})(1-S_{22})-S_{12}S_{21}} \\
Z_{12} &= Z_0 \frac{2S_{12}}{(1-S_{11})(1-S_{22})-S_{12}S_{21}} \\
Z_{21} &= Z_0 \frac{2S_{21}}{(1-S_{11})(1-S_{22})-S_{12}S_{21}} \\
Z_{22} &= Z_0 \frac{(1-S_{11})(1+S_{22})+S_{12}S_{21}}{(1-S_{11})(1-S_{22})-S_{12}S_{21}}
\end{aligned}
\tag{3.7}
$$

8. Use the Eqn. (3.4) to get the results of $L_s^{stub}, C_p^{stub} \text{ and } L_p^{stub}$. From the Eqn.(3.5), we know that L_s^{int} is the majority of the L_R .If necessary, adjust the width, the length of the stub inductor, then repeat step 6 to 8 to get an appropriate inductance value.
9. Based on the above results, use Eqn.(3.5) to calculate the parameters of the unit cell to CRLH TL. Then the corresponding lumped element circuits are built. The dispersion relation diagram of CRLH TL is based on the following equation

$$\beta = -\frac{\varphi(S_{21})}{a} \tag{3.8}$$

With a is the length of the unit cell of CRLH TL and $\varphi(S_{21})$ is the phase value of the transmission coefficient .

10. Verify the transition frequency f_0 where

$$\beta(f_0) = 0 \tag{3.9}$$

If a short section of the microstrip TL is added to each end of the capacitor or inductor and then simulation is done, it is essential to de-embed the component, that is, to subtract the phase shifts due to the additional microstrip line by appropriate reference plane positioning.

3.3 The Initial Model Calculation

In the previous sections, the method to design of the CRLH unit cell is provided. It is clear that the design method is based on the repeated calculations. To create an initial model is an important beginning.

For the interdigital capacitor, we could use Alley's method to calculate an initial value [6]. But his method is based on the charts; here a different method is used [7].

The interdigital capacitor is shown in Fig. 3.3. l is the finger length, w is the width of the microstrip line, s is the finger space, N is the number of finger. ε_e is the dielectric constant of substrate, h. All dimensions are in micrometers.

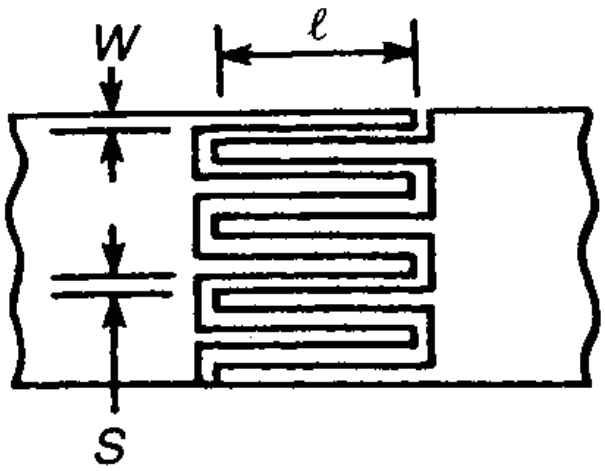

Fig. 3.3 The layout of the Intergidital Capacitor

The equivalent value of the interdigital capacitor is calculated by [8]

$$C(pF) = \frac{\varepsilon_e 10^{-3}}{18\pi} \frac{K(k)}{K^{'}(k)} (N-1)l \qquad (3.10)$$

Where $k = \tan^2(\frac{a\pi}{4b}), a = \frac{w}{2}, b = \frac{w+s}{2}$

the elliptic function

$$\frac{K(k)}{K^{'}(k)} = [\frac{1}{\pi}\ln(2\frac{1+\sqrt{k^{'}}}{1-\sqrt{k^{'}}})]^{-1} \; for \; 0 \le k \le 0.7 \qquad (3.11)$$

$$\frac{K(k)}{K^{'}(k)} = \frac{1}{\pi}\ln(2\frac{1+\sqrt{k^{'}}}{1-\sqrt{k^{'}}}) \; for \; 0.7 \le k \le 1$$

Where $K^{'}(k) = K(k^{'}), \; k^{'} = \sqrt{1-k^2}$

and ε_e is the effective dielectric constant of microstrip line with width W,

$$\varepsilon_e = \frac{\varepsilon+1}{2} + \frac{\varepsilon-1}{2}[\sqrt{(1+12\frac{h}{W})} + 0.04(1+\frac{W}{h})^2] \; for \; \frac{W}{h} < 1$$
$$\varepsilon_e = \frac{\varepsilon+1}{2} + \frac{\varepsilon-1}{2}\sqrt{(1+12\frac{h}{W})} \; for \; \frac{W}{h} > 1 \qquad (3.12)$$

For the stub inductance, the short circuit transmission line can provide the required approximate value [8], $Z(l) = jZ_0 \tan(\frac{2\pi}{\lambda} l)$. Choosing right value of the impedance and the length of the transmission line , we could get the required inductance.

In the beginning of the calculation of the interdigtial capacitor, we have to tried many size parameters to make the calculated value close to the desired one, the layout the corresponding capacitor is made and simulated in ADS. Then S parameters are converted to Y parameters in order to extract the accurate values, as mentioned in the previous two sections. The experiments show that the geometric layout have great effect on the value of the parasitic parameters, so many layouts are simulated and extracted in order to get a design value.

3.4 The Design of the Balanced Unit Cell of CRLH TL

In this section, a balanced unit cell of the CRLH TL, whose transition frequency is 3.850GHz, is built to verify the characteristics of the CRLH TL [1][4], as shown in Fig.3.4. ADS momentum simulations are done to get all the results. The substrate used is Rogers RT/duriod 5880 with dielectric constant $\varepsilon_r = 2.2$ and thickness 1.57mm.

The dimensions of CRLH TL are chosen as follows. For the interdigital capacitor, the finger width is 0.15mm, the gap between the fingers is 0.1mm, the gap at the end of finger is 0.1mm, the length of overlapped region is 4.6mm, the number of finger pairs is 5, the with of interconnect is 0.1mm, the width of the feed line is 2.4mm. For the inductor which is composed of the T section and short-circuit TL, the port width of the T section is

2.4mm, 2.4mm, and 1.1mm separately, the width and length of open-circuit TL are 1.0mm and 5.6mm, the radius of the via is 0.025mm. All the sizes are listed in Table3.1

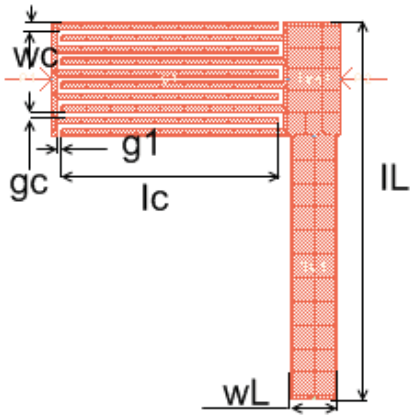

Fig.3.4 The balanced unit cell of CRLH TL

Table 3.1 The size table of the balanced CRLH TL structure (Dimension mm).

wc	gc	lc	g1	IL	wL
0.15	0.1	4.6	0.1	8.0	1.0

The parameters we extracted from the CRLH TL is

$L_R = 2.418nH$ $C_R = 0.444pF$

$L_L = 3.863nH$ $C_L = 0.704nH$

Thus we could get

$f_{sh} = 3.843GHz$
$f_{se} = 3.857GHz$
$f_0 = 3.850GHz$

Though there is a little difference between those three frequencies, taking into account the errors in the calculation procedure, this unit cell is close to a balanced CRLH TL structure.

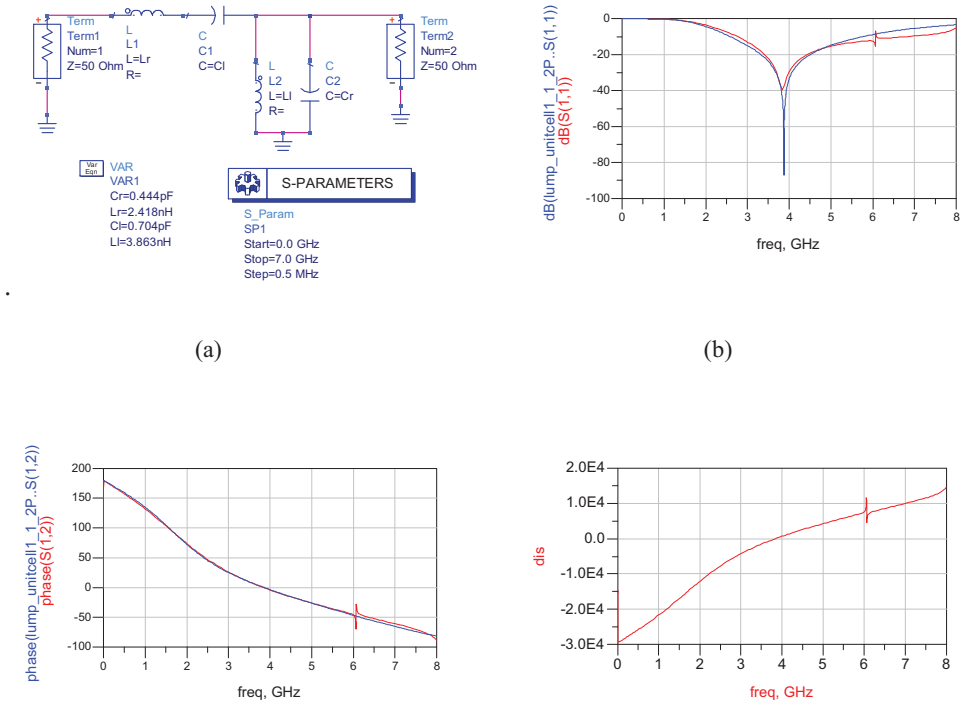

Fig.3.5 The result of balanced CRLH TL, (a) The equivalent lump circuit in Fig 3.4. (b) The magnitude diagram. (The red curve is balanced unit cell; the blue curve is equivalent circuit.) (c) The phase diagram. (The red curve is balanced unit cell; the blue curve is equivalent circuit**).** (d) The dispersion relation of the unit cell of CRLH TL

The balanced CRLH TL is simulated and their result is shown in Fig.3.5. Fig.3.5 (a) shows the equivalent lump circuit of the unit cell in Fig.3.4. From the magnitude diagram

of Fig 3.5.(b) and the phase diagram of Fig3.5.(c), it is clear that the phase diagram of the lump circuit matches pretty well that of the unit cell of the CRLH TL. This verifies that the extraction method gives exact result. Based on Eqn.(3.8), one can get the dispersion relation of the unit cell CRLH TL, as shown in Fig.3.5.(d). The frequencies below the transition frequency belong to the LH range, and that the frequencies above the transition frequency belong to the RH range.

A 4-section cascaded balanced unit cell CRLH TL is simulated in ADS momentum and the corresponding lump equivalent circuits is also simulated. Their S-parameters is shown in Fig.3.6. Fig.3.6.(a) is the S_{11} parameters of 4-section balanced design. Fig.3.6.(b) is the S_{21} parameters of the 4-section balanced design. The properties of the 4-section balanced design behaves like a high-pass filter.

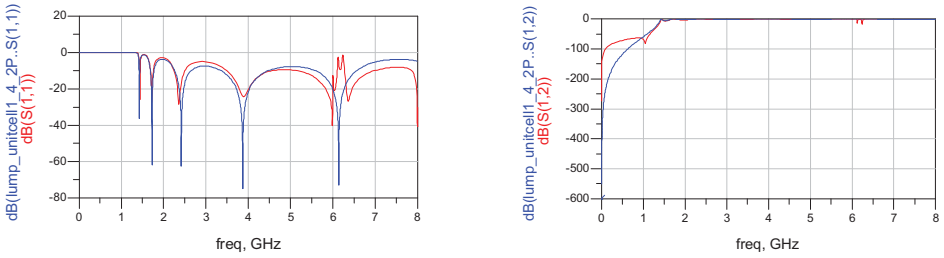

(a) The S11 parameters (b) The S21 parameters

(The red curve is 4-section balanced design. The blue curve is lump equivalent circuit.)

Fig. 3.6 The simulation result of 4-section cascaded balanced design

3.5 The Design of the Unbalanced Unit Cell of CRLH TL

In this section, an unbalanced unit cell of the CRLH TL, whose transition frequency is 3.0GHz, is built to verify the characteristics of the CRLH TL [1][4]. ADS momentum

simulation is done to get all the results. The substrate used is Rogers RT/duriod 5880 with dielectric constant $\varepsilon_r = 2.2$ and thickness 1.57mm.

The size of unbalanced CRLH TL has the following parameters. For the interdigital capacitor, the finger length is 0.3 mm, the gap between the finger is 0.2mm, the gap at the end of finger is 0.2mm, the length of overlapped region is 9.2mm, the number of finger pairs is 5, the with of interconnects is 0.2mm, the width of the feed line is 4.8 mm. For the inductor which is composed of the T section and short-circuit TL, the port width of the T section is 4.8 mm, 4.8 mm, and 2.2 mm separately, the width and length of open-circuit TL are 2.0 mm and 1.2 mm, the radius of the via is 0.1 mm. All the geometrical shape is shown in Fig 3.4 , and those sizes are listed in Table3.2

Table 3.2 The size table of the unbalanced CRLH TL structure (Dimension mm).

wc	gc	lc	g1	IL	wL
0.3	0.2	9.2	0.2	6.0	2.0

The parameters extracted from the CRLH TL is

$$L_R = 3.057nH \qquad C_R = 0.1.223pF$$

$$L_L = 1.380nH \qquad C_L = 1.564nH$$

Thus, the calculated frequencies are then

$$f_{sh} = 3.873GHz$$
$$f_{se} = 2.302GHz$$
$$f_0 = 2.986GHz$$

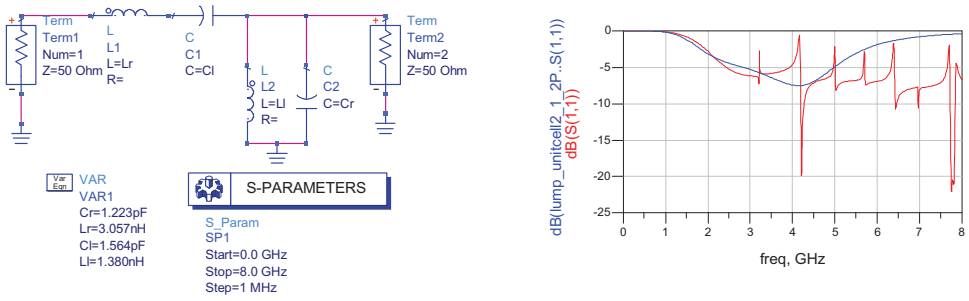

(a)

(b)

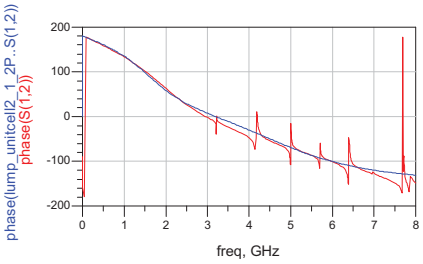

(c)

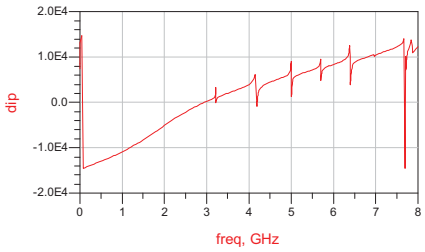

(d)

Fig.3.7 The result of unbalanced CRLH TL. (a) The equivalent lump circuit of unit cell. (b) The magnitude diagram. (The red curve is unbalanced unit cell, the blue curve is equivalent circuit.) (c) The phase diagram. (The red curve is unbalanced unit cell, the blue curve is equivalent circuit.) (d) The dispersion relation of the unit cell of CRLH TL.

The unbalanced CRLH TL is simulated and the results are shown in Fig.3.7. Fig.3.7(a) shows the equivalent lump circuit of the unit cell. As can be seen from the magnitude diagram of Fig 3.7 (b) and the phase diagram of Fig3.7(c), there are many differences between these two diagrams. This may be due to the extraction method being not accurate for the higher frequencies for the same CRLH TL. Basing on the Eqn. (3.8), the

dispersion relation of the unit cell CRLH TL can be obtained as shown in Fig.3.7.(d). We can conclude that the frequencies below the transition frequency belong to the LH range, and that the frequencies above the transition frequency belong to the RH range.

A 4-section cascaded unbalanced unit cell CRLH TL is simulated in ADS momentum, and the lump equivalent circuits is also simulated. Their S-parameters are shown in Fig.3.8. Fig.3.8.(a) is the S11 parameters of 4-section unbalanced design. Fig.3.8.(b) is the S21 parameters of the 4-section unbalanced design. The proprieties of the 4-section balanced design behaves like a high-pass filter.

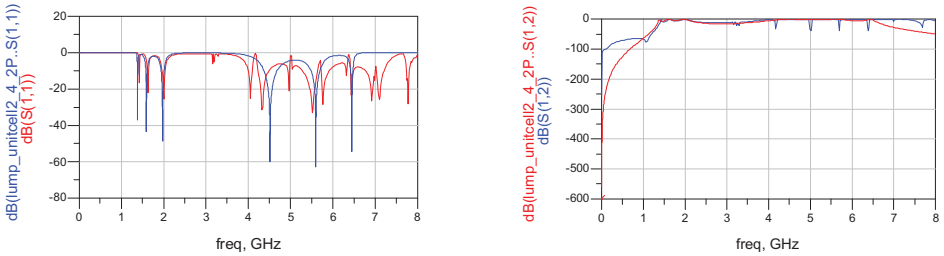

(a) The S11 parameters (b) The S21 parameters

(The red curve is 4-section unbalanced design. The blue curve is lump equivalent circuit.)

Fig. 3.8 The simulation results of 4-section cascaded unbalanced design.

Reference

[1] C. Caloz, A. Sanada, and T. Itoh, "A novel composite right/left-handed coupled-line directional coupler with arbitrary coupling level and broad bandwidth," IEEE Trans. Microwave Theory Tech., vol. 52, pp. 980–992, Mar. 2004.

[2] A. Lai, C. Caloz, and T. Itoh, "Composite Right/Left-handed Transmission Line Metamaterials", IEEE Microwave Magazine, pp. 34-50, September 2004

[3] C. Caloz, A. Sanada, and T. Itoh, "Microwave Circuits Based on Negative Refractive Index Material Structures," 33rd European Microwave Conference – Munich 2003

[4] C. Caloz and T. Itoh, Electromagnetic Metamaterials: Transmission Line Theory and Microwave Applications. New York: Wiley, 2004.

[5] David M. Pozar, "Microwave Engineering", Second Edition, John Wiley & Sons, 1998

[6] Gary D Alley , "Interdigital Capacitors and Their Application to Lumped-Element Microwave Integrated Circuits" ," IEEE Trans. Microwave Theory Tech., vol. 18, pp. 1028–1035, Dec. 1970.

[7] Inder Bahl, Prakash Bhartia, "Microwave Soldid State Circuits Design" New York: Wiley, 2003

[8] Reinhold Ludwig, Pavel Bretchko, "RF Circuit Design: Theory and Application" New Jersey, Prentice Hall,2000

Chapter 4

Antenna Application of CRLH TL

4.1 The Tag Antenna Design Based on the CRLH TL

Our goal is to design an RFID tag antenna operating at the frequency of range 902~930MHz, which is the commercial RFID frequency band. The center frequency of the tag antenna is 915MHz. Our aim is to design a commercially affordable antenna. It is important to fabricate the antenna small, cheap, simple and affordable. At the same time, the characteristics of the tag antenna also should include acceptable gain and radiation efficiency.

Though there have many design examples for the tag antenna.[1][2][3],at the same time, more design example from the website could be found, and most of those designs have been used commercially. For most of those antennas, they are implemented by the single layer PCB antenna on plastic substrate without ground plane. These antennas don't work well in most cases. When those antennas are mounted on containers with metallic contents, such as on the surface of the box with metal cans inside, those antennas do not work properly. The background metallic containers modify the antenna radiation parameters.

Thus a compact antenna with ground plane is our design goal. At the same time, the small antenna should be cheap, simple and affordable and with acceptable gain and radiation efficiency.

The Zeroth-Order Resonator antenna, as described in Section 2.6, also could be used as the antenna[4][5][6]. The ZOR unit cell is composed of the series interdigital capacitor and a shunt meander-linear inductor connected to a metal patch, which is 1-D CRLH unit cell structure. The metal patch provides a capacitor to the ground. The ZOR antenna based 2-D CRLH is also practical [7].

Initially, it is reasonable to replace the metal patch with a via to connect to the ground due to the fact that the metal patch provides a "virtual ground" at the operating frequency. At the same time, the single section antenna seems to be best due to its size

But this simple initial concept does not work too well. At the designed frequency, the CRLH unit cell composed of interdigital capacitor and meander-line inductor with via connected to the ground does not resonate when the energy is fed directly from a single input port through the transmission line.

It is not clear why the initial thought does not work in practice as expected. A reasonable explanation is that the structure of the transmission line connected directly to the ZOR destroys the resonant structure. In order to verify this new assumption, a ZOR with new coupling structure is made, as shown in Fig.4.1.

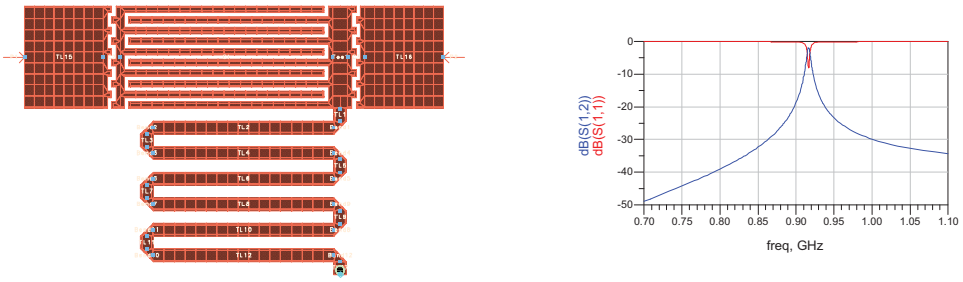

(a) The layout of the ZOR with two coupling ports (b) The simulation result of (a)

Fig.4.1 The layout and result of ZOR with two coupling ports

Fig.4.1 proves our assumption that the best way to resonate the ZOR CRLH antenna is to couple energy into it through a gap.

The gap in the transmission line could be regarded as a Π network composed of capacitors [8]. Similar to the Π network shown in Section 3.1 and Section 3.2, it is easy to extract the accurate capacitor parameters.

Two types of ZOR CRLH antenna designs are provided: balanced and unbalanced design and they are summarized in the following two sections.

4.2 The Unbalanced ZOR CRLH antenna

In this section, an unbalanced ZOR CRLH unit cell is designed, as shown in Fig.4.2. and ADS momentum simulation is done to get all the results. The substrate used is Rogers RT/duriod 5880 with dielectric constant $\varepsilon_r = 2.2$ and thickness 1.57mm.

For the interdigital capacitor: the finger length is 0.3mm, the gap between the finger is 0.2mm, the gap at the end of finger is 0.2mm, the length of overlapped region is 9.2mm, the number of finger pair is 5, the with of interconnect is 0.2mm, the width of the feed line is 4.8 mm; the inductor which is composed of the T section and short-circuit TL, the port width of the T section is 2.4mm, 4.8mm, and 0.7 mm separately, the width and length of meander-line are 0.6 mm and 8.5 mm, the width of the bend is 0.6mm, the radius of the via is 0.2mm.

The dimensions (mm) of CRLH TL are given in Table 4.1,

Table 4.1 The dimensions of unbalanced CRLH TL

lc	wc	gc	g1	Nc	IL	gL	wL	NL
9.2	0.2	0.2	0.2	5	8.5	0.6	0.6	7

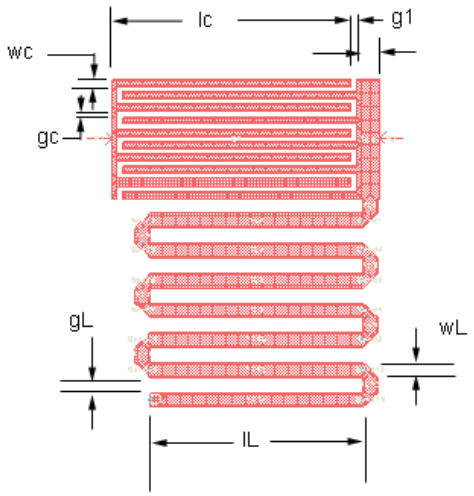

Fig.4.2 The unbalanced ZOR CRLH unit cell

The parameters extracted from the CRLH TL are

$$L_R = 3.470nH \qquad C_R = 1.323pF$$

$$L_L = 23.525nH \qquad C_L = 1.247nH$$

The corresponding frequencies are:

$$f_{sh} = 0.902GHz$$
$$f_{se} = 2.420GHz$$
$$f_0 = 1.477GHz$$

From the relation between the resonant frequencies, we know that the above CRLH antenna is an unbalanced design.

Naturally, a gap is added to couple energy into the balanced ZRO CRLH antenna, as shown in Fig.4.3 (a). Like cascaded CRLH TL unit cell, the ZRO CRLH unit cell also can be cascaded with only one input port. The resulting S11 parameters are shown in Fig.4.3.(b).

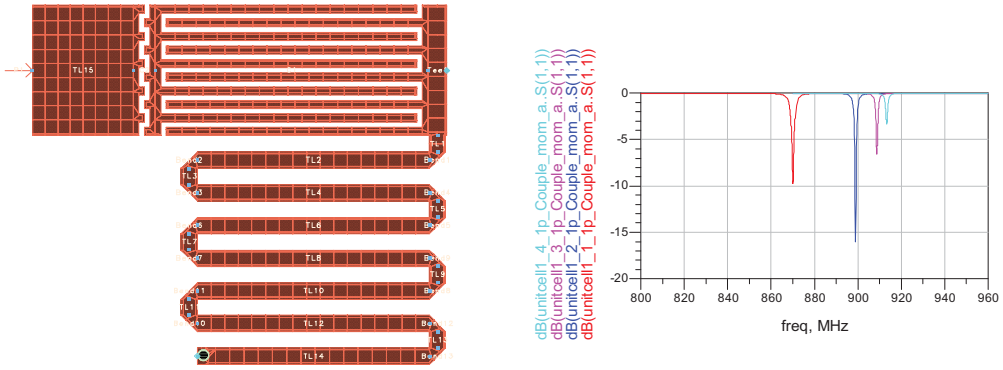

(a) The layout of the ZOR CRLH antenna (b) The S_{11} parameters of different cells number

(The red curve is the 1-cell ZOR ,the blue curve is the 2-cell ZOR, the pink curve is the 3-cell ZOR, the indigotic curve is the 4-cell ZOR)

Fig. 4.3 The layout and the simulation result of the unbalanced ZOR CRLH antenna

From the S11 parameter data of the ZOR CRLH antenna, the ZOR antenna has a different resonant frequency. It is due to the capacitor effecting of the gap and could be easily corrected by adjusting the length of meander line .At the same time, when the number of cell is 2, the ZRO CRLH antenna has the best VSWR, which means the maximum energy is radiated in this case.

Adjusting the length of meander line of each ZRO antenna cell, the corresponding results are shown in Fig.4.4.

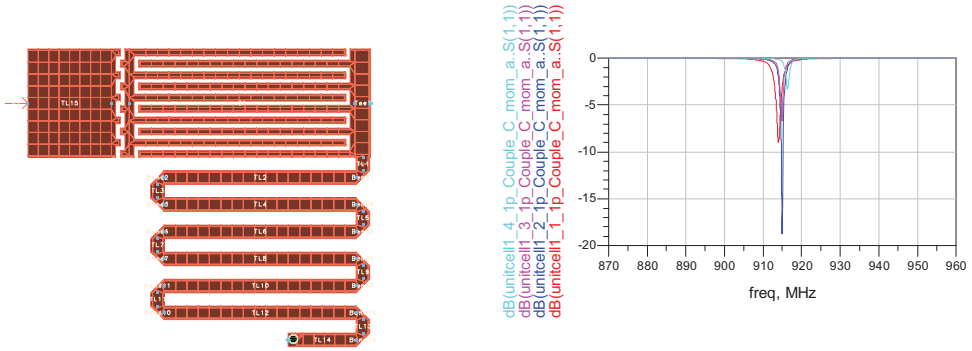

(a) (b)

Fig. 4.4 The layout and the simulation result of the unbalanced ZOR CRLH antenna with adjusted meander length . (a) The layout of the ZOR CRLH unit cell with adjusted meander length.(b) The S11 parameters of different cells number ZOR CRHL antenna. (The red curve is the 1-cell ZOR ,the blue curve is the 2-cell ZOR, the pink curve is the 3-cell ZOR, the indigotic curve is the 4-cell ZOR)

The radiation characteristics of the 4 unit cell ZOR CRLH antenna are shown as Fig.4.5.

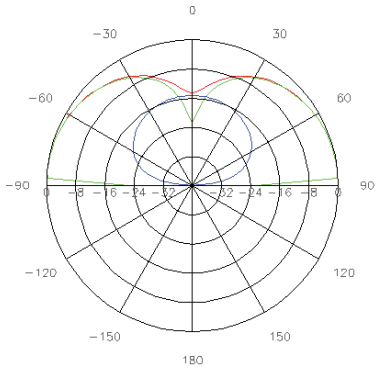

Power radiated (watts)	0.0001932436858	
Effective angle (degrees)	237.61	
Directivity (dB)	4.814749436	
Gain (dB)	4.12288757	
Maximum Intensity	4.659833422e-005	
Angle of U Max (theta, phi)	81.00	213
E(theta) Max (mag, phase)	0.1873522364	147.0905919
E(phi) Max (mag,phase)	0.003025649721	-129.0709393
E(x) Max (mag,phase)	0.02445811325	-36.75033766
E(y) Max (mag,phase)	0.01642968195	-24.07639013
E(z) Max (mag,phase)	0.1850456195	-32.90940812

Fig. 4.5 The radiation pattern of the unbalanced multi-cell ZOR CRLH antenna

From the above simulation results, some conclusion can be summarized as follows;

- The cell number of the ZOR antenna does not effect on the radiation pattern. The radiation range is above the antenna plane and the maximum radiation appears away from the antenna broadside plane and the minimum appears at the broadside plane.

- The cell number of the ZOR antenna has negligible effect on the directivity, but the larger the number, the higher is the gain, which means the efficiency improves with the increase of the cell number. But it is also noted that the radiated power is increased with the increase of cell number due to the S11 parameter decrease.

4.3 The Balanced ZOR CRLH Antenna

In this section, a balanced ZOR CRLH unit cell is designed as shown in Fig.4.6. ADS momentum simulations are done to get all the results. The substrate used is Rogers RT/duriod 5880 with dielectric constant $\varepsilon_r = 2.2$ and thickness 1.57mm.

The dimension of the balanced CRLH TL is listed in Table 4.2.

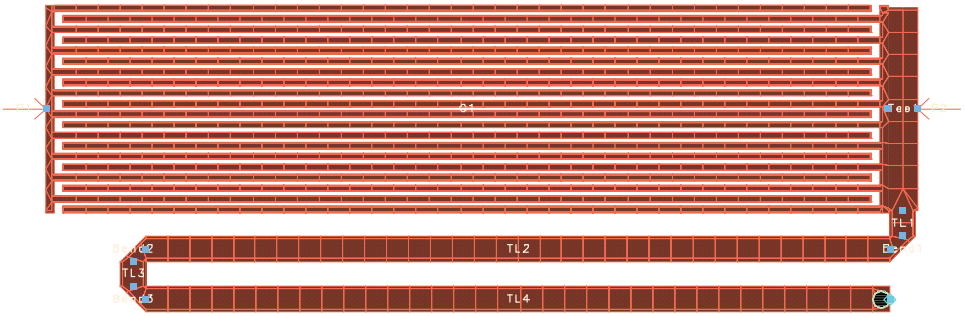

Fig.4.6 The balanced ZOR CRLH unit cell

Table 4.2 The dimension (mm) of balanced CRLH unit cell

lc	wc	Gc	g1	Nc	IL	gL	wL	NL
19	0.15	0.1	0.2	5	17.5	0.6	0.6	2

The parameters of CRLH TL are as follows: for the interdigital capacitor, the finger length is 0.15mm, the gap between the fingers is 0.1mm, the gap at the end of the fingers is 0.2mm, the length of overlapped region is 19mm, the number of finger pairs is 10, the with of interconnect is 0.2mm, the width of the feed line is 4.8 mm; the inductor which is composed of the T section and short-circuit TL, the port width of the T section is 2.4mm,

4.9mm, and 0.7 mm separately, the width and length of meander-line are 0.6 mm and 17.5 mm, the width of the bend is 0.6mm, the radius of the via is 0.2mm.

The parameters we extracted from the CRLH TL are

$$L_R = 5.307nH \qquad C_R = 2.167pF$$

$$L_L = 14.226nH \qquad C_L = 5.771nH$$

Thus we could get

$$f_{sh} = 0.905GHz$$
$$f_{se} = 0.909GHz$$
$$f_0 = 0.907GHz$$

Though there is a little difference between those three frequencies, taking into account the accuracy of errors in the calculation procedure, we still think that this unit cell is a balanced CRLH TL.

Similarly, a gap is added to couple energy into the balanced ZRO CRLH antenna, as shown in Fig.4.7 (a). Like cascaded CRLH TL unit cell, the ZRO CRLH unit cell also could be cascaded with only one input port. The S11 parameters also shown in Fig.4.7(b).

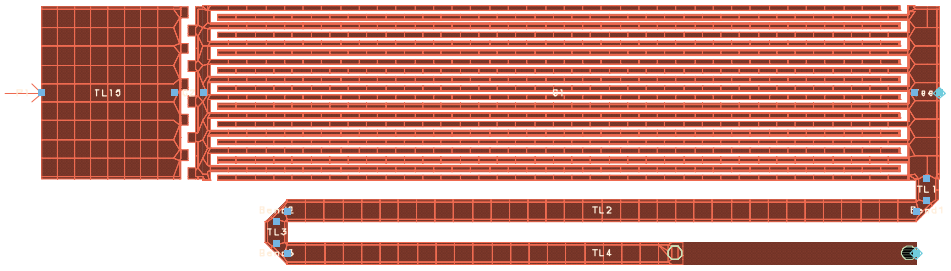

(a) The layout of the ZOR CRLH antenna

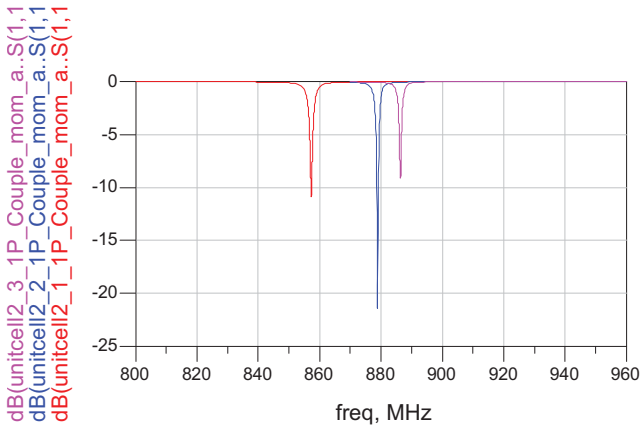

(b) The S11 parameters of different cells l ZOR CRHL antenna

(The red curve is the 1-cell ZOR ,the blue curve is the 2-cell ZOR, the pink curve is the 3-cell ZOR)

Fig. 4.7 The layout and the simulation result of the balanced ZOR CRLH antenna

From the S_{11} parameters of the ZOR CRLH antenna, the multiple ZOR antennas have different resonant frequencies. It is due to the capacitor effecting the gap and could be easily corrected by adjusting the length of meander line .At the same time, when the number of cells is 2, the ZOR CRLH antenna has the best VSWR, which means the maximum energy is radiated in this case.

The effect of adjusting the length of the meander line of each ZOR antenna cell, the corresponding results are shown in Fig.4.8.

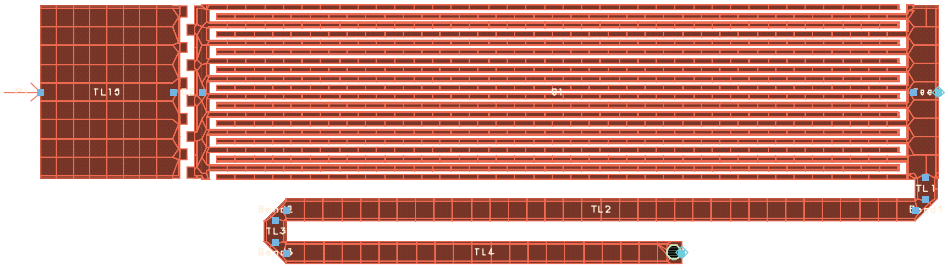

(a) The layout of the ZOR CRLH unit cell with adjusted meander length

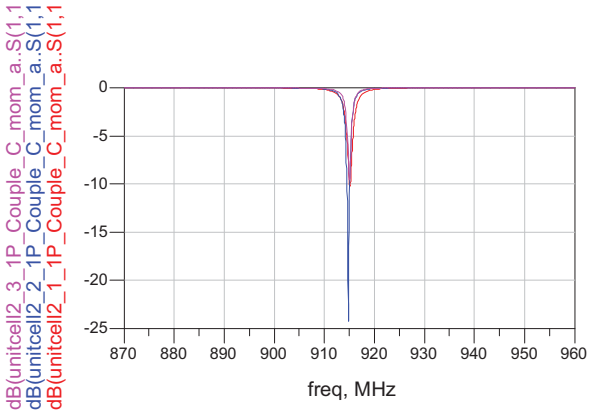

(b) The S_{11} parameters of different cells l ZOR CRHL antenna

(The red curve is the 1-cell ZOR ,the blue curve is the 2-cell ZOR, the pink curve is the 3-cell ZOR)

Fig. 4.8 The layout and the simulation result of the balanced ZOR CRLH antenna with adjusted meander length

The simulated radiation characteristics of the 3 unit cell ZOR CRLH antenna are shown in Fig.4.9.

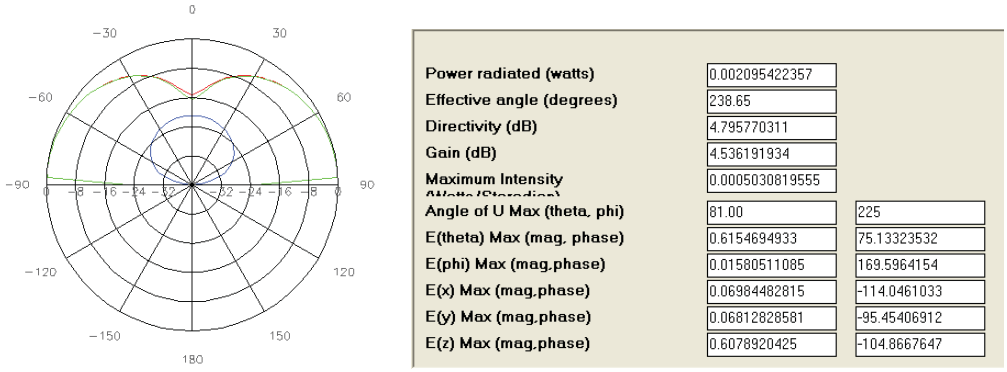

Fig. 4.9 The radiation pattern of the balanced 3 unit cell ZOR CRLH antenna

From the above simulation results, and compared with the simulation results in Section 4.2, it is clear that two types of CRLH antennas have similar radiation patterns. It seems that the balanced CRLH antenna have better radiation efficiency.

Reference

[1] S. Lahiri, RFID Sourcebook, IBM Press, 2006

[2] R. Want, RFID Explained: A Primer on Radio Frequency Identification Technologies. Moragn & Claypool Publisher, 2006

[3] K. Finkenzeller, RFID Handbook: Radio-Frequency Identification Fundamental and Application, John Wiley & Son,1999

[4] A. Sanada, C. Caloz, and T. Itoh, "Zeroth order resonance in composite right/left-handed transmission line resonators," in Proc. Asia-Pacific Microwave Conf., vol. 3, pp. 1588–1592. Seoul, Korea, 2003.

[5] A. Sanada, K.Murakami, I.Awai, C. Caloz, and T. Itoh, " A planear zeroth-order resonator antenna using a left-handed transimission line," in Proc. European Microwave Conf. pp.1341-1344, Amsterdam, Nerherlands, Apr. 2004.

[6] A.Sanada, K.Murakami, S.Aso, H.Kubo, and I.Awai, "A via-free microstrip left-handed transmission line," IEEE MTT-S Digest, pp.301-304, Fort Worth, Jun.2004.

[7] C. J. Lee, K.M.K.Leong, and T. Itoh, "Composite right/left-handed transmission line based compact resonant antenna for RF module integration," IEEE Trans. Antennas Propagat., vol. 54, pp. 2283–2291 Aug. 2006.

[8] David M. Pozar, "Microwave Engineering", Second Edition, John Wiley & Sons, 1998

Chapter 5

Additional Simulations and Experimental Measurements

5.1 Patch Antenna Design

For comparison, a half-wave patch antenna using the same substrate, Rogers RT/duriod 5880 with dielectric constant $\varepsilon_r = 2.2$ and thickness 1.57mm, is designed as shown in Fig.5.1.

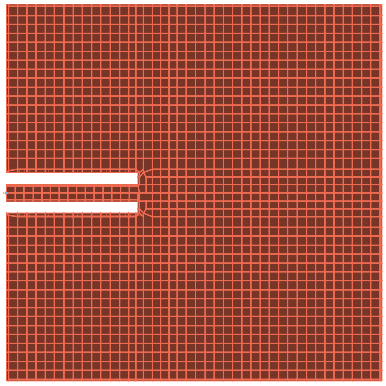

(a) The layout of the half-wave patch antenna

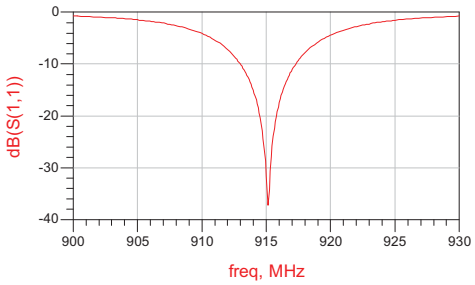

(b) The S11 parameters of half-wave patch antenna

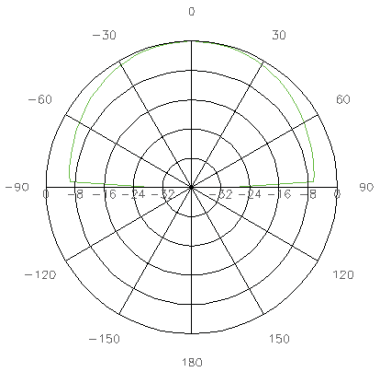

(c) The radiation pattern of the half-wave antenna

Power radiated (watts)	0.002206532314	
Effective angle (degrees)	128.52	
Directivity (dB)	7.483714559	
Gain (dB)	6.944404445	
Maximum Intensity	0.0009837208669	
Angle of U Max (theta, phi)	0.00	0
E(theta) Max (mag, phase)	0.8609268523	27.31284445
E(phi) Max (mag,phase)	0	-180
E(x) Max (mag,phase)	0.8609268523	27.31284445
E(y) Max (mag,phase)	0	0
E(z) Max (mag,phase)	0	-180

(b) The radiation parameters of half-wave antenna

Fig.5.1 The matched half-wave patch antenna

5.2 Comparisons of ADS Simulation Results

Comparisons are made between the half-wave patch antenna and those ZOR CRLH antennas based on the ADS simulation results, which are all operated at 915MHz and fabricated on the same substrate. All those parameters for the ZOR CRLH antennas are shown in Section 4.3, 4.4 and 5.1. During the simulation, the metal conductor using both the perfect conductor and the real metal copper is taken into account, and the results are summarized in Table 5.1.

Table 5.1 The simulation results of the designed antennas

Parameters of antenna		Size (mm)	Directivity (dB)	Efficiency （perfect conductor）	Efficiency (copper)
Half-wave patch antenna		110×110	6.94	89.1%	79.4%
Balanced ZOR CRLH antenna	1-cell	25×7.2	4.83	40.4%	3.82%
	2-cell	45.5×7.2	4.80	71.3%	7.52%
	3-cell	66.0×7.2	4.80	95.5%	10.61%
	4-cell	86.5×7.2	4.80	96.5%	13.74%
Unbalance ZOR CRLH antenna	1-cell	15.2×13.2	4.80	59.1%	3.53%
	2-cell	25.9×13.2	4.80	78.7%	5.40%
	3-cell	36.6×13.2	4.80	86.4%	7.76%
	4-cell	47.3×13.2	4.83	40.4%	9.88%

Conclusion drawn from these results can be summarized as follows.

1. ***Size comparisons.*** The size of the half-wave patch antenna is 110×110mm. While, for those balanced ZOR antennas, the size is 25×7.2mm, 45.5×7.2 mm , 66×7.2mm and

86.5×7.2mm.And for those unbalanced ZOR antennas, the size is 15.2×13.2mm, 25.9×13.2 mm , 36.6×13.2mm and 47.3×13.2mm. The ZOR CRLH antennas have 94% less antenna area compared with the half-wave patch antenna.

2. ***Radiated power***. When all the input ports are fed by the same sinusoidal wave, with a peak-to-peak magnitude of 1V, the half-wave patch antenna has the biggest capability to radiate power, and its value is 0.0022W. The 3-cell balanced ZOR CRLH antenna has the second highest power radiated of 0.0021W.

3. ***Effective angle***. The effective Half-Power angle of the half-wave patch antenna is 128˚, which is far narrower than that of the ZOR CRLH antenna 238˚.

4. ***Directivity***. The directivity of the half-wave patch antenna is 6.94dB, with the different unit numbers, the directivity of the balanced and unbalanced ZOR CRLH antenna is around 4.80dB.

5. ***Efficiency***. In the simulation with the perfect conductor, the half-wave antenna has an efficiency 89.1%, while the efficiency of the balanced ZOR CRLH antenna is 40.4%,71.3% ,95.5% and 96.5% and that of unbalanced ZOR CRLH antenna is 35.5%, 59.1%, 78.7% and 86.4%. In the simulation with the real copper conductivity, the half-wave antenna has an efficiency 79.4%, while the efficiency of the balanced ZOR CRLH antenna is 3.82%, 7.25% and 10.61% and 13.74% with the increase of the unit number .And the efficiency of the unbalanced ZOR CRLH antenna is 3.53%, 5.40%, 7.76% and 9.88% respectively. This indicates that the real ZOR antenna has poor radiation efficiency, but its efficiency is increases with increasing unit number.

6. ***Radiation patter***n. Both antenna types radiate above their antenna plane, but their radiation patterns are different. The half-wave patch antenna radiates largest at the

direction vertical to the plane (broadside), while the ZOR CRLH has greatest radiation near parallel to the antenna ground (endfire).

From the above comparison of the simulation results, it is clear that the ZOR CRLH antennas have unique radiation characteristics. Due to the small size, the ZOR CRLH with a ground plane is a possible choice for RFID tag antenna.

5.3 Experiment results.

In order to verify the ADS simulation results, previously designed antennas are fabricated and measured in the lab.

Due to the slim finger and the narrow spacing between the fingers of the interdigital capacitor, the technique of photolithography is required to ensure the accuracy of the fabrication process. We chose the Datak negative acting liquid photo resist ER-8 and the corresponding developer.

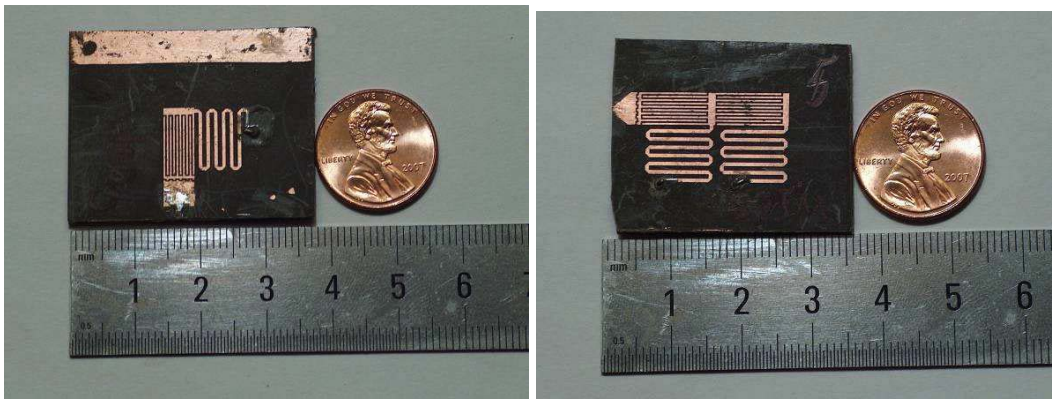

(a) The 1 unit cell unbalanced ZOR antenna (b) The 2 unit cell unbalanced ZOR antenna

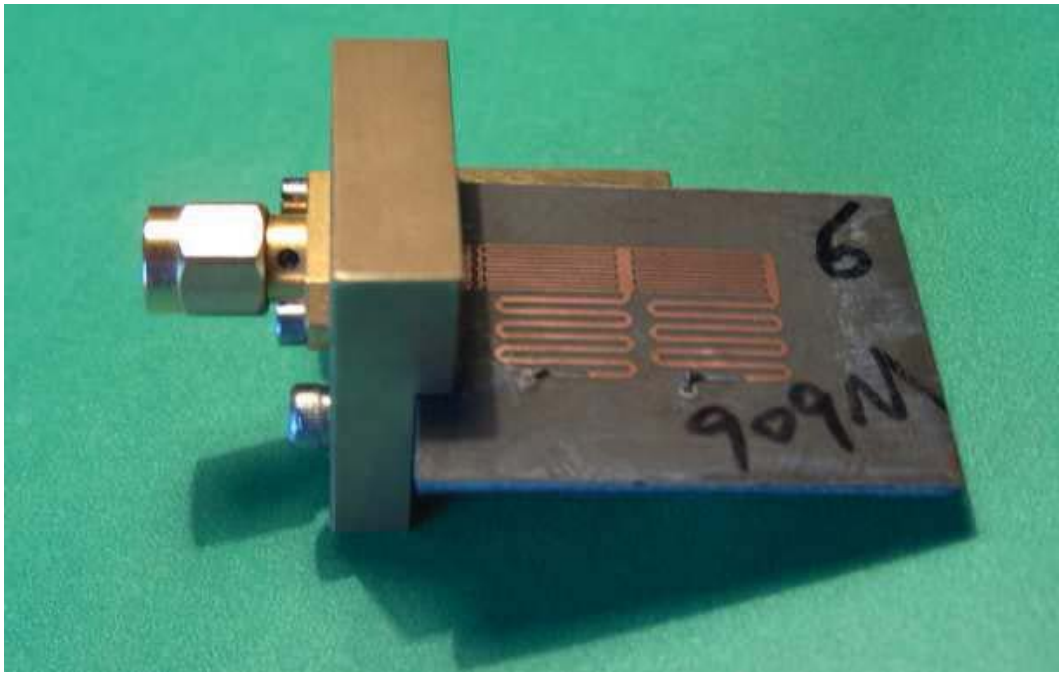

(c) The test holder with a 2 unit cell unbalance ZOR antenna

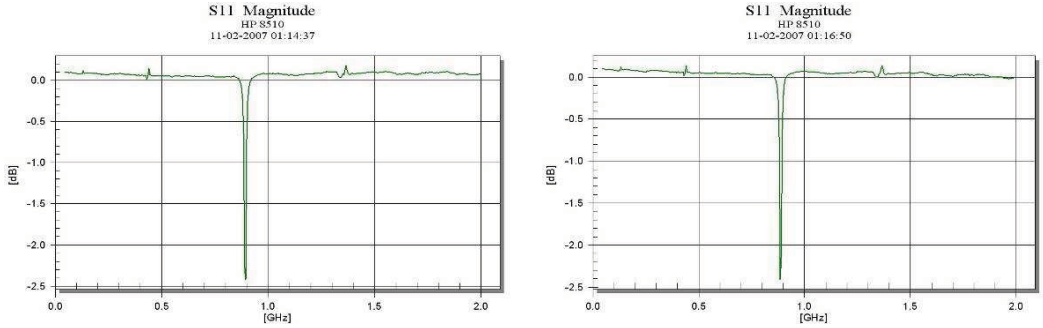

(d) The S11 parameter of 1 unit cell antenna (e) The S11 parameter of 2 unit cell antenna

Fig. 5.2 The layout and the test results of the 1& 2 unit cell unbalanced ZOR antenna

After several experiments, 1 unit cell and 2-cell unbalanced ZOR CRLH antennas are implemented and shown in Fig.5.2 (a) and (b). During the test, the antenna is mounted on the test hold, shown in Fig. 5.2 (c). Their measured S11 parameters are shown in Fig.5.2 (d) and (e).

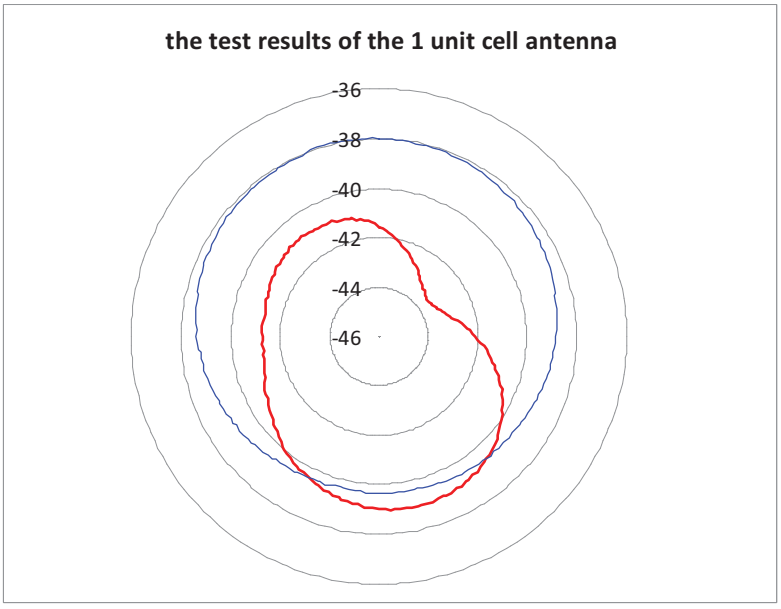

(a) The test results of the 1 unit cell ZOR antenna

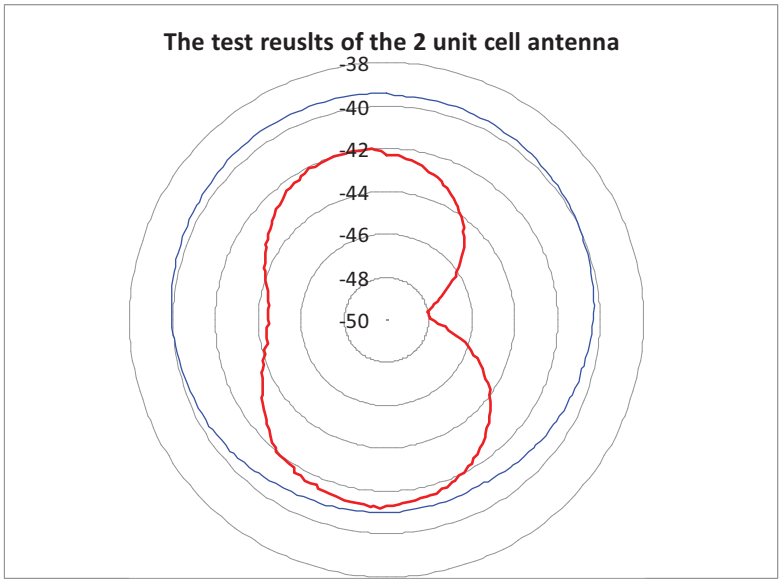

(b) The test results of the 2 unit cell ZOR antenna

(The top summit is the 0 degree, the initial point of test process, the test holder rotate clockwise, same with the figure. The red line is the endfire test results and the blue line is the broadside test results. For the endfire test, the initial point is the position that the ZOR unit cell is laid between the input port and the transmitter antenna. For the broadside test, the initial point is the position the ZOR unit cell facing the transmitter antenna.)

Fig. 5.3 The radiation pattern of the ZOR antenna.

The radiation pattern of the CRLH antenna was tested in Microwave and Millimeter Lab at University of Cincinnati.

Inside of the microwave chamber, the transmitter antenna, a quarter wave monopole antenna with a big ground plane is mounted and connected to the signal synthesizer on one side, on the other side, the receiver antenna, the CRLH antenna with the antenna holder is connected to the power meter and mounted on a test platform, which is rotatable and is driven by a stepper motor. A VEE program is executed to control the signal synthesizer, the power meter and the stepper motor. At the same time, the results from the power meter is recorded.

Two radiation faces are measured: endfire and broadside.

The test results of the radiation pattern are shown in Fig 5.3. Compared with the simulation results shown Fig 4.12, we could get some interesting points:

The measured S11 parameters are not as good as the simulation results in ADS . A possible explanation is the electromagnetic effect that metal block at the antenna input port and the way the antennas are mounted on the holder for test measurements. As can be seen from the Fig.5.2c, when the antenna is rotated in the plane of the antenna, the coax-adapter metal is protruding above the antenna plane and may affect the radiation pattern measured when this part of the fixture faces the receiving system.

Because of the fixture, the measured radiation patterns are different from the simulation results in ADS. It is also because in ADS, the simulations are based on the assumption that the antennas have infinite ground planes and radiation results in the ADS simulation results only in the broadside.

5.4 Effect of the Ground size

In ADS momentum simulation processing, the ground plane of the antenna is assumed to be infinite. But in realization of the actual antenna it is not. In this section, we simulate 1 unit cell ZRO antenna at 915 MHz with different ground sizes in HFSS software. It will be assumed that the square ground size increases and the 1 unit cell antenna is located in the center of the ground size

When the ground size is 40×40mm, the radiation pattern is shown in the Fig.5.4.

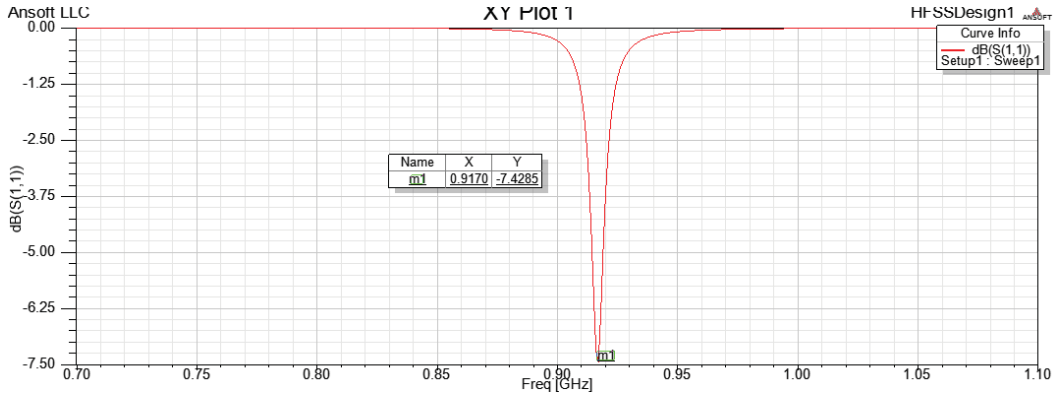

(a) The S11 parameters of the 1 unit cell Antenna with the ground size 40×40mm.

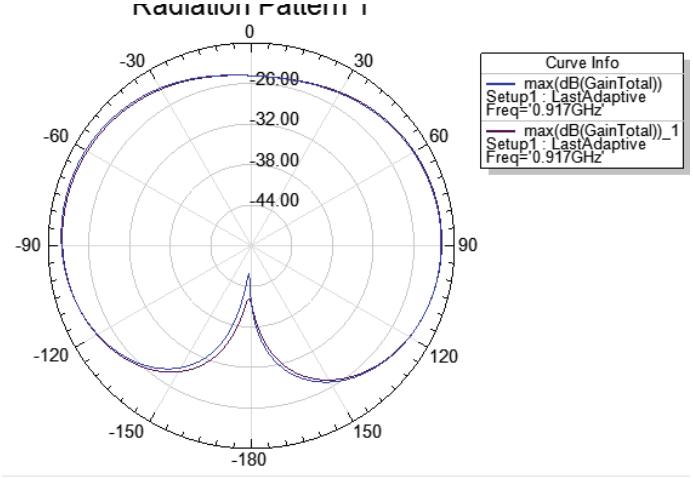

(b) The radiation pattern of the 1unit cell Antenna with the ground size 40×40mm.

Fig.5.4 The parameters of the 1unit cell Antenna with the ground size 40×40mm.

When the ground size is 500×500mm, the radiation pattern is shown in the Fig.5.5.

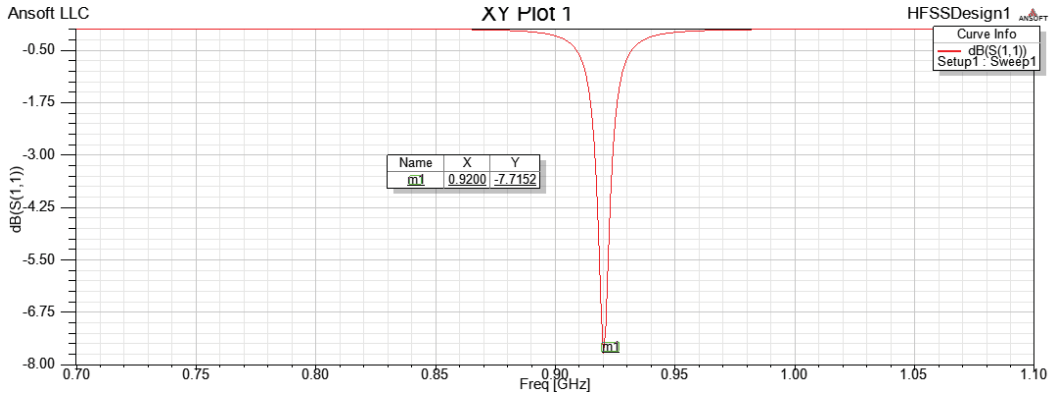

(a) The S11 parameters of the 1unit cell Antenna with the ground size 500×500mm.

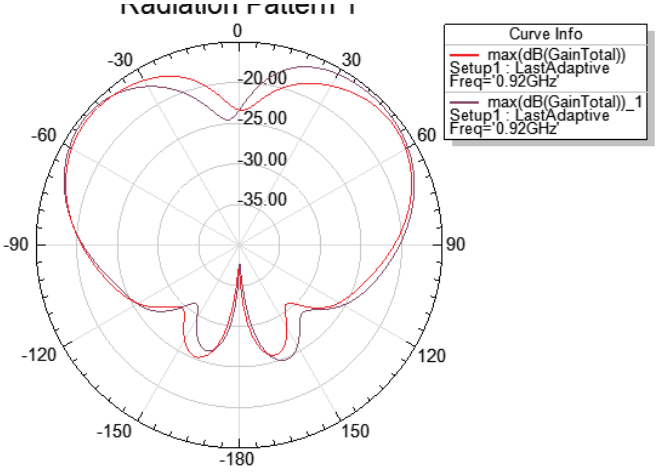

(b) The radiation pattern of the 1unit cell Antenna with the ground size 500×500mm.

Fig.5.5 The parameters of the 1unit cell Antenna with the ground size 500×500mm.

From Fig.5.4 and Fig.5.5, it is clear that the ground size has great effect on the resonant frequency and the radiation pattern and gain. Table 5.2 shows that relation between the ground size and the peak frequency of S11 parameters.

For the 1 unit cell CRLH antenna, with the increase of the ground size, the peak frequency in the S11 parameters changes in an unpredicted way.

The radiation power increase in the direction above the ground plane and decrease in the direction under the ground plane with the bigger ground size.

For an infinite ground plane, all power is radiated above the ground plane and as expected no radiation is observed under the ground plane. So this is in compliance with the ADS simulation results shown in Fig 4.12,.

Table 5.2 the relation between the peak frequency of S11 and the ground size

Size of the ground (mm)	The peak frequency of S11 (GHz)
40×40	0.917
50×50	0.917
60×60	0.922
80×80	0.896
100×100	0.910
200×200	0.905
300×300	0.868
400×400	0.850
500×500	0.920

5.5 The Metal Sidewall Effects

The 1 unit cell antenna is located in the center of the ground plane and the ground plane size is 40×40mm.

The metal sidewall may be used to prevent radiation from the sides of the dielectric substrate. The metal sidewall is shown in Fig 5.6. In this case, the 1 unit cell antenna is mounted inside of an open metal box which is composed of sidewalls and the ground plane.

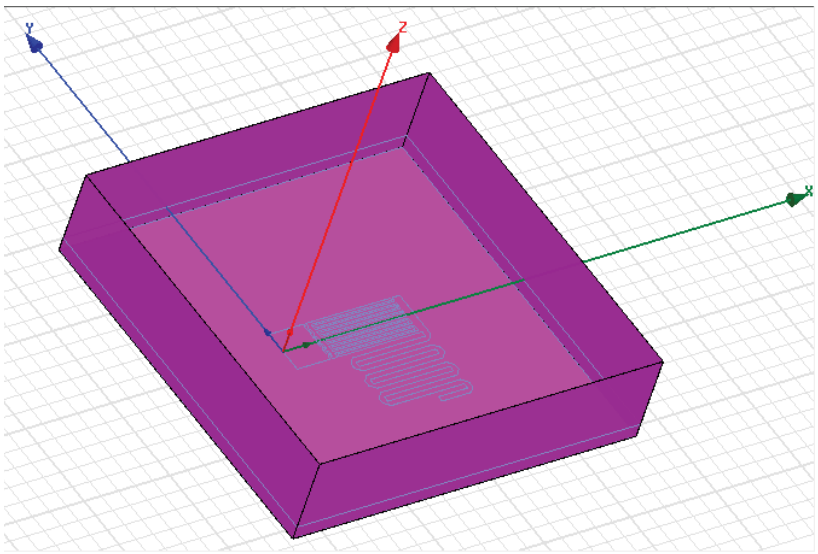

Fig 5.6 The 1 unit cell antenna with the metal sidewall.

Considering the gain and directivity into account, the efficiency of the antenna can be calculated. In fact, through these, some interesting simulation results are obtained. These results are shown in Fig. 5.7 to Fig. 5. 11, and in Table 5.3.

Table 5.3 the simulation results of the 1 unit cell antenna with different height of the metal sidewall

The height of the metal sidewall(mm)	The peak frequency of S11 (GHz)	The difference between Gain and Directivity (dB)	The efficiency
0	0.902	10.6	8.8%
1.57	0.908	11.2	7.6%
3.14	0.908	11.7	6.8%
10	0.900	15.7	2.7%
40	0.909	37.9	0.002%
80	0.892	65.0	0
165	0.888	121.0	0

When the metal side wall is removed, the result is shown in Fig 5.7

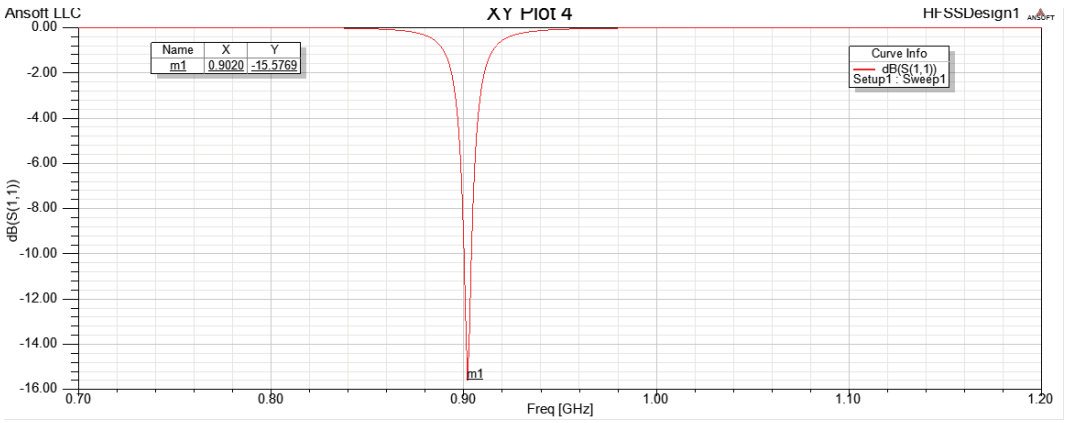

(a) The S11 of 1 unit cell antenna with no mental sidewall.

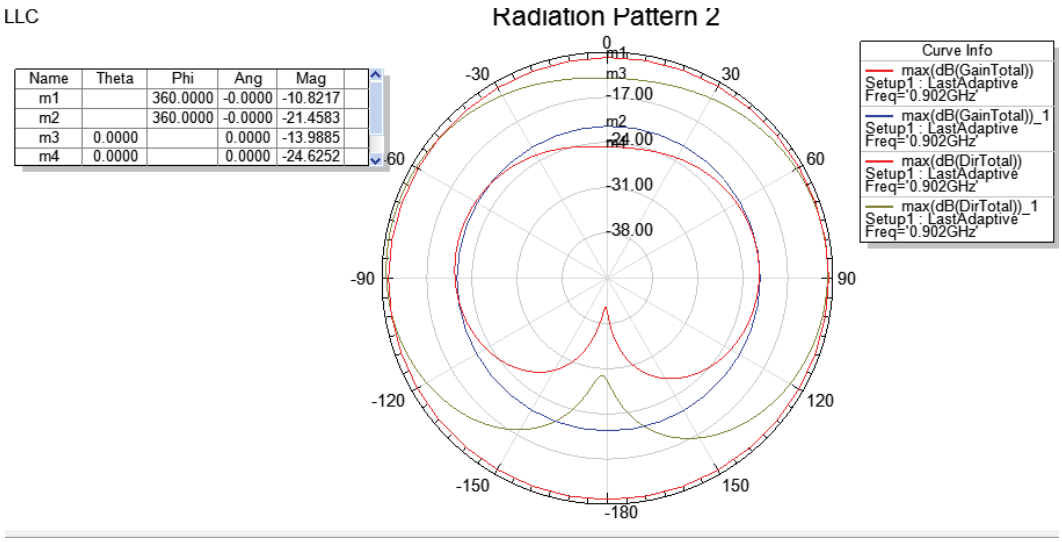

(b) The radiation pattern of 1 unit cell antenna with no metal sidewall.

Fig.5.7 The parameters of the 1 unit cell antenna with no metal sidewall.

The radiation pattern of 1 cell antenna with 1.57mm metal box (the same height of substrate) is shown in Fig 5.8

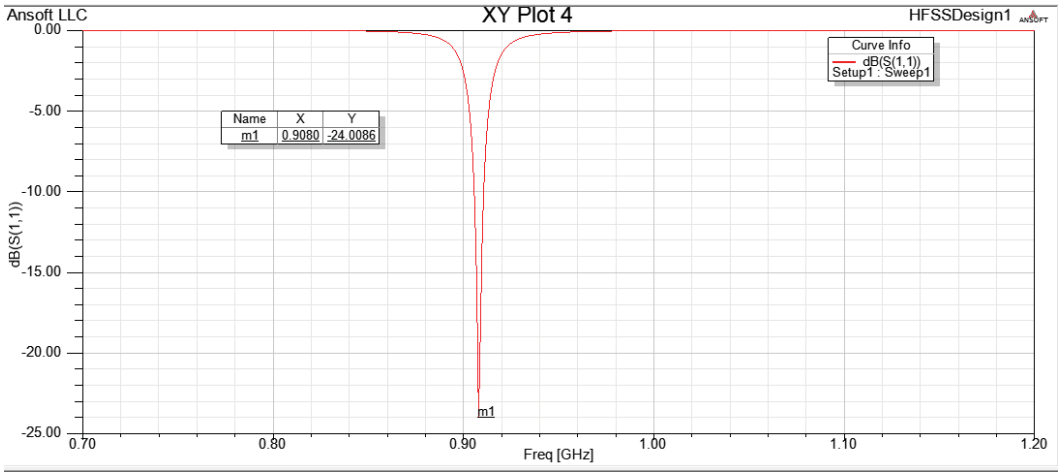

(a) The S11 of 1 unit cell antenna with the metal sidewall 1.57 mm high

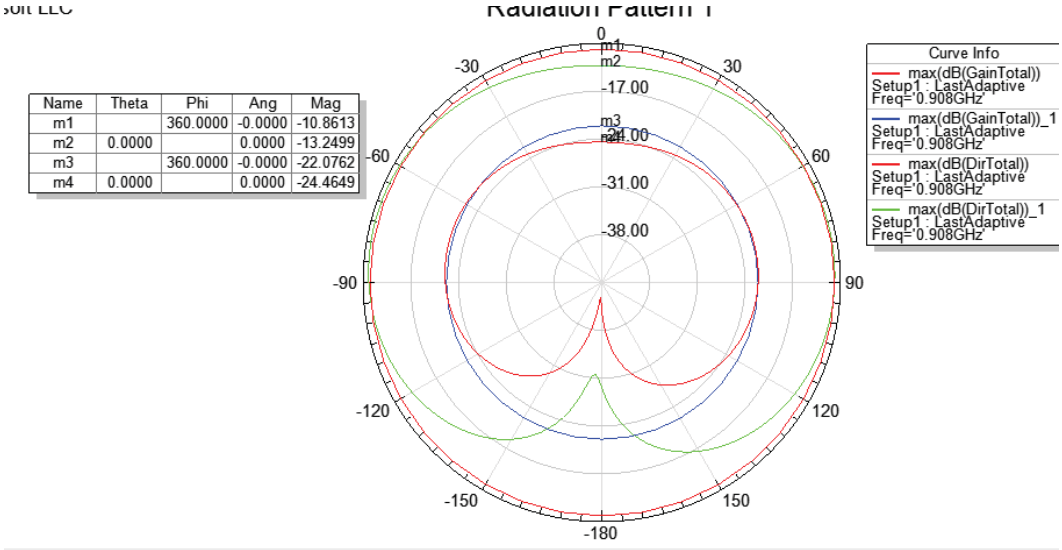

(b) The radiation pattern of 1unit cell pattern with 1.57 mm metal sidewall

Fig. 5.8 The parameters of 1 unit cell antenna with 1.57mm metal sidewall

The radiation pattern of 1 cell antenna with a metal sidewall 10 mm high is shown in Fig. 5.9

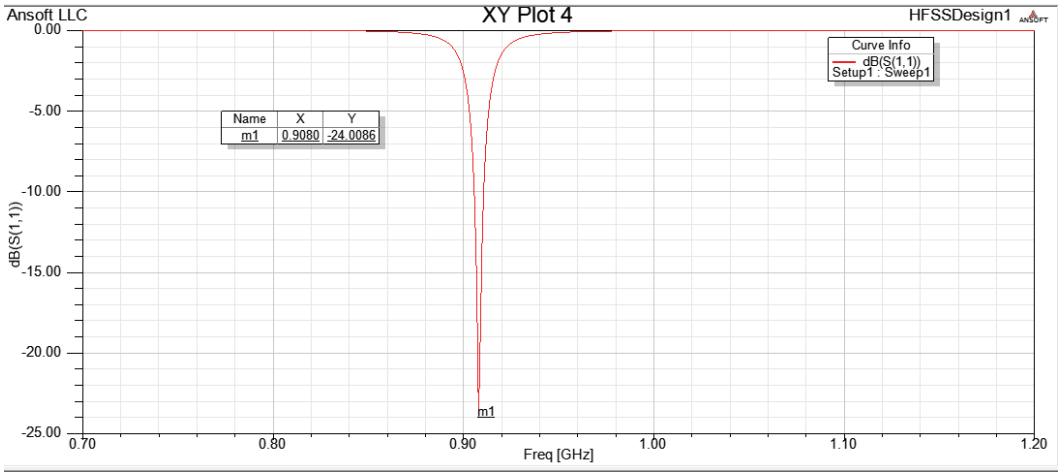

(a) The VSWR of 1 unit cell antenna with the metal sidewall 10 mm high

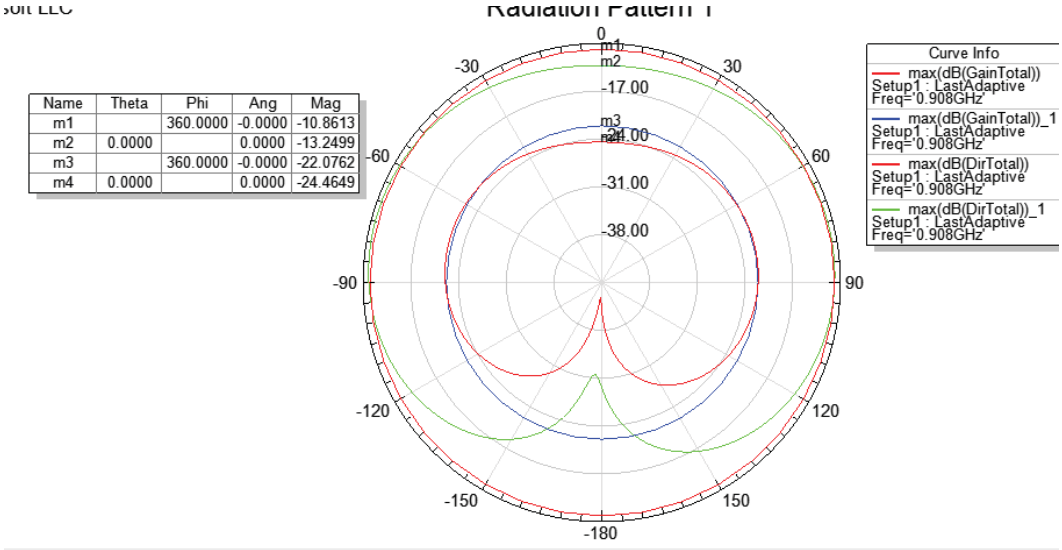

(b) The radiation pattern of 1unit cell pattern with the metal sidewall 10 mm high

Fig. 5.9 The parameters of 1 unit cell antenna with the metal sidewall 10mm high

The radiation pattern of 1 cell antenna with a metal sidewall 40 mm high is shown in Fig 5.10

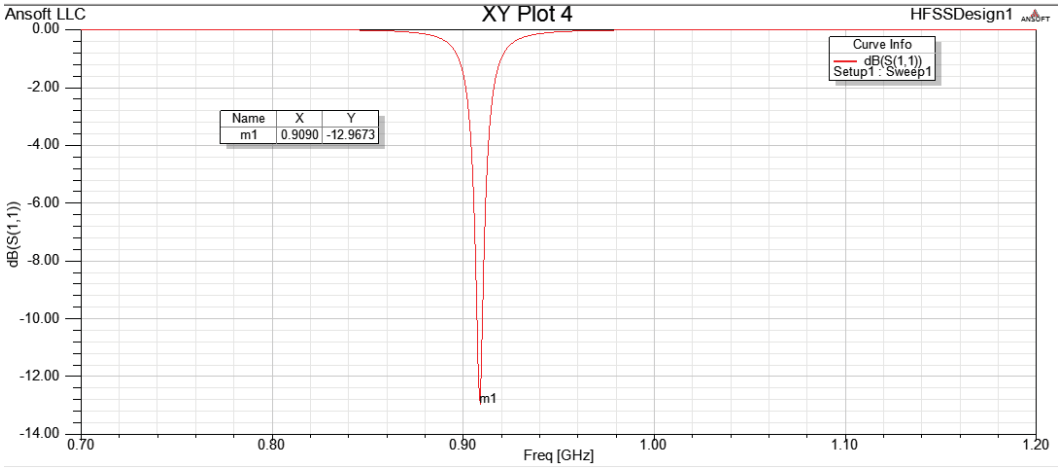

(a) The S11 of 1 unit cell antenna with the metal sidewall 40 mm high

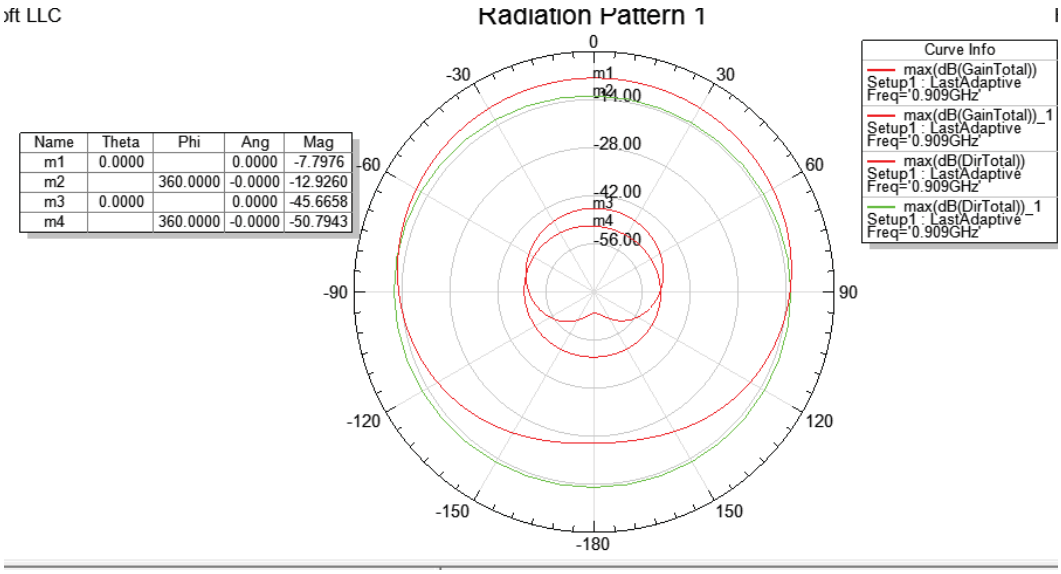

(b) The radiation pattern of 1unit cell pattern with the metal sidewall 40 mm high

Fig. 5.10 The parameters of 1 unit cell antenna with the metal sidewall 40mm high

The radiation pattern of 1 cell antenna with a metal sidewall 80 mm high is shown in Fig 5.11

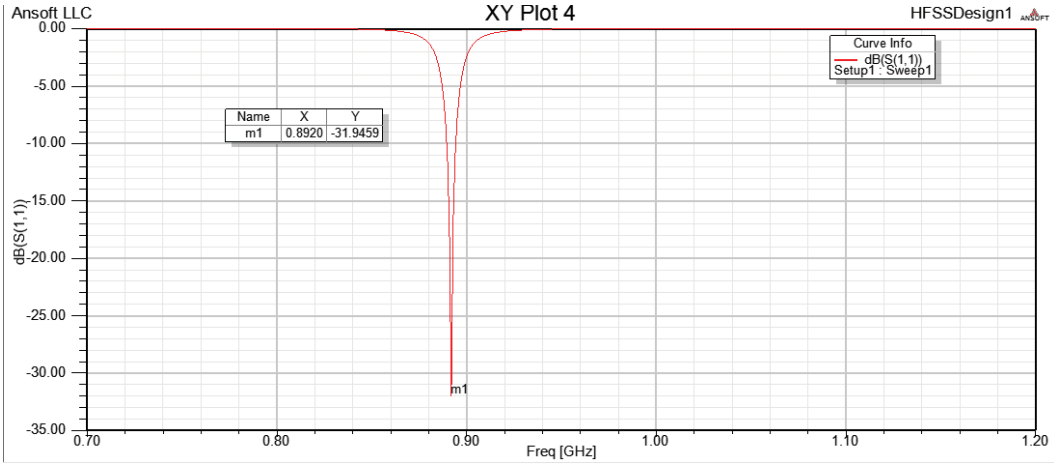

(b) The S11 of 1 unit cell antenna with the metal sidewall 80mm high

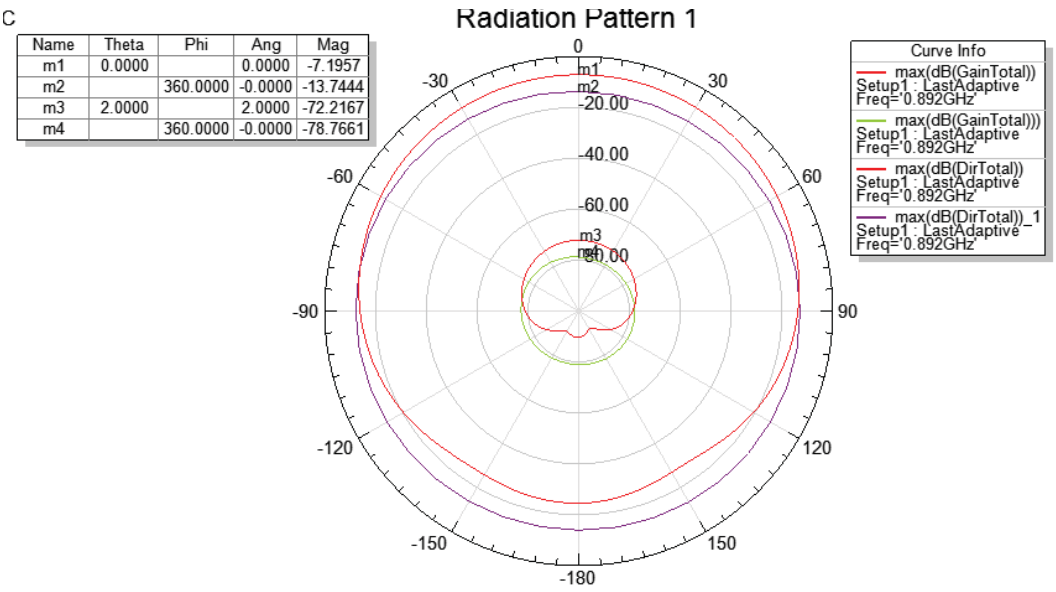

(b) The radiation pattern of 1unit cell pattern with the metal sidewall 80 mm high

Fig. 5.11 The parameters of 1 unit cell antenna with the metal sidewall 80mm high

Some conclusions:

1) The results in Fig. 5.7 are different from that in the Fig. 5.4. It is because the size of the ground in Fig. 5.7 is a little bigger than that in Fig. 5.4. It seems that the peak frequency of S11 is sensitive to the size of the antenna ground.

2) The metal sidewall changes the peak frequency of S11 parameters

3) The height of the metal sidewall has negative effect on the radiation pattern and the efficiency. The higher the mental sidewall, the less power is radiated in the vertical direction. So is the efficiency. It is clear that the electromagnetic field radiated from the 1 unit cell antenna is confined in a limited space above ground plane. The increase of the metal can be treated as a waveguide and the antenna radiation properties are affected by the wave guiding effects of the side walls.. According to calculation, the cutoff frequency of 40mm square waveguide is 3.75GHz. At 915MHz, the propagation is actually attenuated with the mental sidewall. So the higher the sidewall, the less power is radiated.

4) In HFSS simulation for the 1 cell antenna without the mental box, its efficiency is about 8%. In the ADS, the efficiency of 1 cell antenna is about 4%, as shown in Table 5.1. The reasonable explanation to this difference is that the ADS simulation is based on the infinite ground plane.

5.6 Further Research Suggestions.

Compared with the traditional patch antennas, the ZOR CRLH antennas is not dependent on the physical restrictions of the resonant frequency, but on the values of the

series capacitors and the shunt inductors. So the ZOR CRLH antenna is implemented in a small size.

Based on the theory of the CRLH TL, the resonant frequencies of the ZOR CRLH antenna are dependent on the value of the parameters L_L, C_R and L_R, C_L. The simulation results verify the theories of the CRLH TL and the ZOR CRLH antenna .As expected, the ZOR CRLH antennas have compact sizes, easy to match and good radiation patterns.

In order to design the ZOR CTLH antenna operating at lower frequency range, such as HF, VHF or UHF, bigger values of parameters are required. Unfortunately, The CRLH TL technology based on the interdigital capacitor and short stub inductor just could provide the limited values of the capacitances and inductances. Some new technologies, such as the 2-D CRLH structure based on the metal insulator metal (MIM) with high dielectric constant and thin substrate height, can generate the higher values. More attention should be paid in this area.

Experiments show that the 1 unit cell CRLH antenna has a poor efficiency. The improvement of the efficiency is the most important part to its commercial usage. The possible ways to improve the performance of these antennas are: 1) using them at higher frequencies and 2) incorporate multi-cell antennas